Coordination Chemistry Reviews 431 (2021) 213760

Contents lists available at ScienceDirect

Coordination Chemistry Reviews

journal homepage: www.elsevier.com/locate/ccr

Review

The shape of porphyrins

Christopher J. Kingsbury [a], Mathias O. Senge [a,b,*]

[a] School of Chemistry, Trinity Biomedical Sciences Institute, 152-160 Pearse Street, Trinity College Dublin, The University of Dublin, Dublin 2, Ireland
[b] Institute for Advanced Study (TUM-IAS), Technical University of Munich, Focus Group – Molecular and Interfacial Engineering of Organic Nanosystems, Lichtenberg-Str. 2a, 85748 Garching, Germany

ARTICLE INFO

Article history:
Received 18 November 2020
Accepted 20 December 2020
Available online 22 January 2021

Dedicated to the memory of Prof. John A. Shelnutt

Keywords:
Porphyrins
X-ray crystallography
Normal-coordinate analysis
Structure-property relationship
Macrocyclic ligands
Principal component analysis

ABSTRACT

Porphyrin molecules are a widely exploited biochemical moiety, with uses in medicinal chemistry, sensing and materials science. The shape of porphyrins, as an aromatic unit, is reductively imagined to be approximately flat, with regular, rigid shape, owing to the popular depiction as a simplified skeletal model. While this regular conformation does exist, the array of substitution patterns in synthetic porphyrins or interactions with the apoprotein in biochemical moieties often induce distortions both in-plane and out-of-plane. Structural deviation reduces symmetry from the ideal D_{4h} and can introduce changes in the physical and electronic structure; physical changes can introduce pockets for favorable intermolecular interactions, and electronic distortion can introduce new electronic transitions and properties. A quantification of porphyrin distortion is presented based on the Normal-coordinate Structural Decomposition method (NSD) pioneered by Shelnutt. NSD transforms crystallographically-determined atomic positions of each porphyrin into a summation of common concerted atom vectors, allowing for quantification of porphyrin anisotropy by symmetry. This method has been used previously for comparison of small data sets of synthetic and biological porphyrins. In the twenty-five years since the method was pioneered, the volume and variety of available crystal structure data has ballooned, and data analysis tools available have become more sophisticated, while the method has languished. Using modern data-science methods, clusters of porphyrin distortions are grouped to show the average effect that a substitution pattern has on porphyrin shape. Aiming to provide an overview on the shape and conformation of these key macrocycles we here provide context to the strategies employed for introducing porphyrin distortion and to provide a quantitative comparative basis for analysis of novel structures. This is achieved by demonstrating that porphyrin molecules often have a predictable NSD pattern, and therefore solid-state conformation, based on chemical arguments. This quantification allows for assessment of predicted structures and forms the basis of a symmetry-by-design motif for a range of porphyrinoids. A modernized computer program used in this structural determination is provided for analysis, with this treatise acting as a guide to the interpretation of results in new structure determinations. New features include simple report generation, prediction of symmetry and assessment of cluster behavior for a range of porphyrin moieties, as well as convenient plotting functions and data reductions.

Contents

Abbreviations: CCDC, Cambridge Crystallographic Data Centre; CSD, Crystal Structure Database; Hb, hemoglobin; HOMO, highest-occupied molecular orbital; KDE, Kernel Density Estimation; OEP, 2,3,7,8,12,13,17,18-octaethylporphyrinato; OETPP, 2,3,7,8,12,13,17,18-octaethyl-5,10,15,20-tetraphenylporphyrinato; NSD, Normal-coordinate structural decomposition; TPP, 5,10,15,20-tetraporphyrinato; Pc, Phthalocyaninato; PDB, Protein Data Bank.

* Corresponding author at: School of Chemistry, Chair of Organic Chemistry, Trinity Biomedical Sciences Institute, 152-160 Pearse Street, Trinity College Dublin, The University of Dublin, Dublin 2, Ireland.

E-mail address: sengem@tcd.ie (M.O. Senge).

https://doi.org/10.1016/j.ccr.2020.213760
0010-8545/

1. Introduction

Tetrapyrrole molecules such as porphyrins (**1**), chlorins, bacteriochlorins and corrinoids are the colors of life – arguably the most widely known and exploited biochemical and synthetic macrocyclic chelate [1–3]. Porphyrins and chlorins are essential for plant and animal life, playing essential roles in respiration [4], photosynthesis [5], and electron transport [6]. Porphyrin materials are characterized by strong and tunable light absorption and allow for modulation of their excited state and catalytic properties. Readily accessible through stepwise and synchronous condensation routes [7–9], synthetic porphyrins are used as sensor components [10], photodynamic therapy medicines [11,12], photocatalysts [13], and solar energy conversion dyes [14,15], to name only a few. Well-developed synthetic modification techniques allow for introduction of a wide variety of modifications to the core and periphery of the macrocyclic systems (Fig. 1) [7,8,16–22].

Simple synthetic porphyrins, such as (5,10,15,20-tetraphenyl porphyrinato)zinc(II) (**1**, M = Zn(II), [23]) or (2,3,7,8,12,13,17,18-octaethylporphyrinato)zinc(II) (**2**, M = Zn(II) [24]), are highly symmetrical and approximately planar, as observed from crystal structure analysis. The shape of porphyrin molecules is reductively imagined to be similarly symmetrical and invariant and, while many have approximately regular structure, the combination of steric, bonding, and electronic effects can induce variations on this core pattern. The simplest variation is the modification of the core – metal centers which have an optimal coordination environment smaller or larger than that provided by the planar macrocycle induce distortion in the macrocycle to elicit the preferred coordination environment. The classic case here are the Ni(II) porphyrins (e.g., **2**, M = Ni(II) [25]) which predominantly adopt the ruffled out-of-plane geometry, as shown in Fig. 2 [26].

Biogenic tetrapyrroles, chief among them the variants of the heme and phytochlorin subunits, show a range of distortions from planar, regular structure [27–29]. These molecular shapes alter the properties of pyrrolic molecules to perform a range of functions within the natural world, including photosynthesis, reversible binding of oxygen and electron transfer [30–34]. The alteration of shape of a ligand by protein environment, a form of allostery, is a method of fine-tuning reactivity [35,36]. For example, the shape change from domed to planar in hemoglobin (Hb) upon cooperative oxygen-binding having been an extensively studied case of this effect [37,38]. A comparison of the conformation of the heme unit in the two crystal structures of this classic is shown in Fig. 3 [39,40].

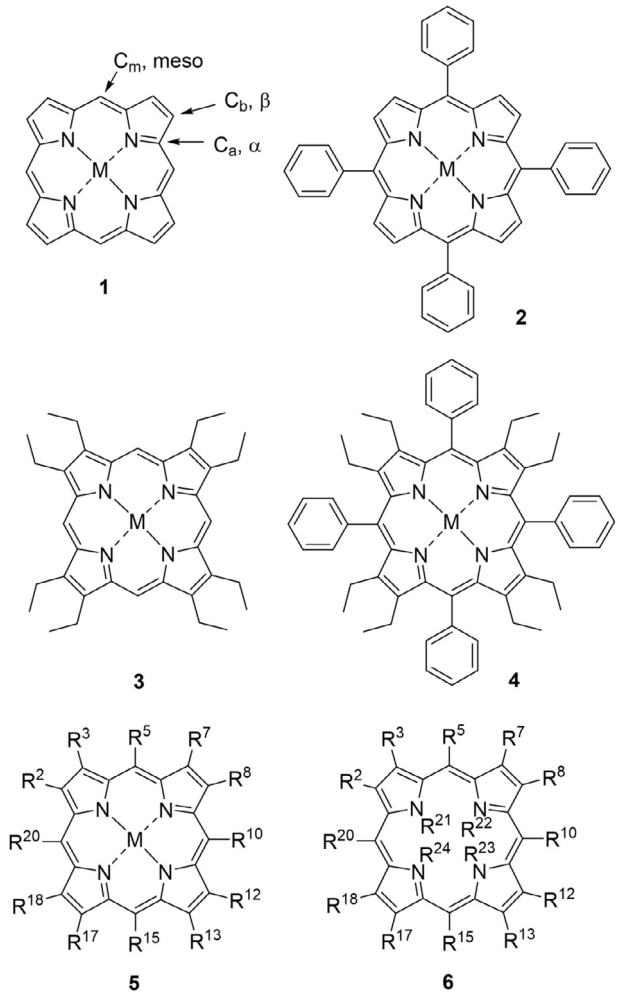

Fig. 1. Standard substituent pattern in core and/or peripherally substituted porphyrins and numbering scheme used herein.

Stone and Fleischer, in their groundbreaking paper on the distortional profiles of non-planar porphyrins, such as the porphyrin diacids (see later in Fig. 10), noted that out of plane distortion were significantly more accessible than in-plane distortion for these aromatic units [41]. Descriptive terms such as saddle, ruffled, twisted,

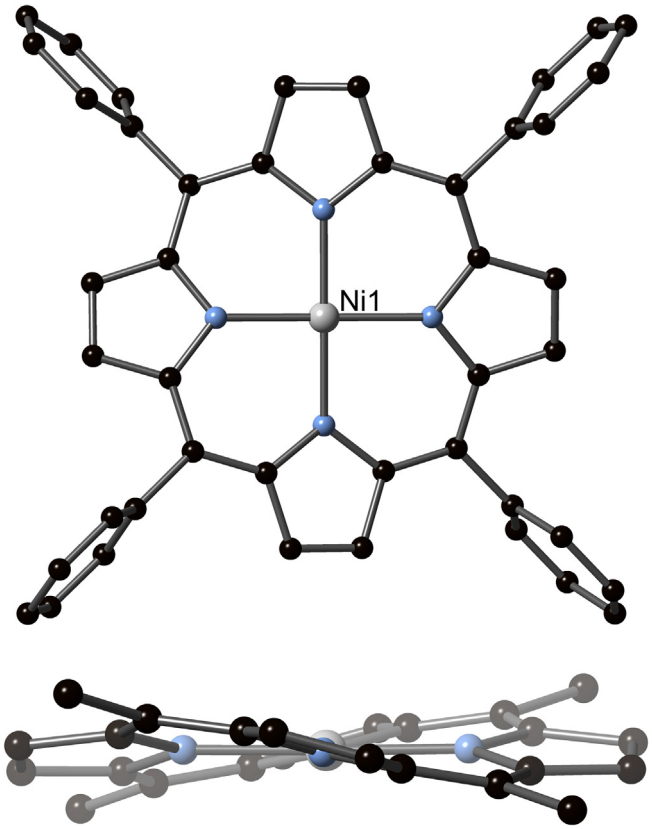

Fig. 2. Top and side view of the ruffled porphyrin core in the crystal structure of (5,10,15,20-tetraphenylporphyrinato)nickel(II) [**1**, M = Ni(II)]. Images generated from CCDC No. 1,320,805 CSD code ZZZUUC01 [25].

etc. were used to describe the various conformations over the years and first systematically applied by Scheidt in his fundamental studies on metalloporphyrin stereochemistry [42,43]. The out-of-plane distortions of porphyrin macrocycles were observed to be broadly correlated with the lowest frequency calculated vibrational modes of each irreducible representation of the D_{4h} idealized symmetric group, and are given trivial names such as saddle (B_{2u}), ruffle (B_{1u}), dome (A_{2u}) and wave (E_g) [29,43,44], Illustrative examples of these main distortion modes are shown in Fig. 4.

Strategies to yield porphyrins with significant deviations from planarity include core, peripheral and electronic manipulation, redox reactions, as well as exocyclic bridging or strapping, and interfacial manipulation. More detail on the synthetic and structural aspects of nonplanar porphyrins and the concomitant alterations in chemical reactivity, electrochemistry and (photo)physical properties [45] can be found in respective reviews [46,47]. For example, the out-of-plane shape of a porphyrin molecule has a strong effect on porphyrin electronic structure [45,48,49]. Using the four-orbit model of porphyrin electronic HOMO/LUMO states presented by Gouterman [50], the molecular orbitals responsible for the absorption spectra of the porphyrin chromophore derivative exist on the ligand surface of the porphyrinoid molecule, i.e. localized to the macrocycle. In the simplest representation, out of plane distorted porphyrins show red-shifted Q- and Soret bands, in line with destabilization of the HOMO a_{1u} and a_{2u} orbitals, especially for ruffled and saddled porphyrins [49–53]. Additionally, satellite peaks are observed when molecular distortion and orbital symmetry correspond, such as for the domed porphyrin series (A_{2u} distortion) with the a_{2u} HOMO. To highlight, overcrowding of the porphyrin periphery, such as in the classic chimera of TPP and OEP skeletons 2,3,7,8,12,13,17,18-octaethyl-5,10,15,20-tetraphenylporphyrin (**4**, M = 2H; H_2OETPP), yields a porphyrin molecule distorted significantly from planar structure, usually in a saddle shape, as demonstrated in Fig. 5 [54]. Later we will describe in detail means how to assign numerical values to these distortional profiles.

Next to their relevance as biomimetic compounds out-of-plane distorted porphyrins such as OETPP and other saddle-distorted porphyrinoids have recently found renewed interest as organocatalysts [55,56] due to their ability to facilitate N–H···X interactions and to use the porphyrin macrocycle as a ligand [57]. Non-planar porphyrins are especially interesting as sensor components, due to the conformational and prototropic changes on the binding of analytes resulting in measurable photophysical change [10,58,59] and have also been used as scaffolds for accessing specific porphyrin atropisomers [60].

Out-of-plane distortion of the porphyrin macrocycle has been characterized well, the more subtle shifts in atom positions which occur parallel to the mean plane of the macrocycle (in-plane distortions) have been less interrogated. The substitution patterns around a porphyrin can access lower symmetry of a macrocycle in a complimentary fashion to the out-of-plane structure, which allows for fine-tuning of electronic structure, and access to chiral aromatics. Substitution patterns such as 5,15-diarylporphyrin series stretch the 5,15-axis of the porphyrin and compress the 10,20-axis, rectangularizing the square porphyrin moiety [61–67]. This structural distortion is complementary to an equivalent electronic

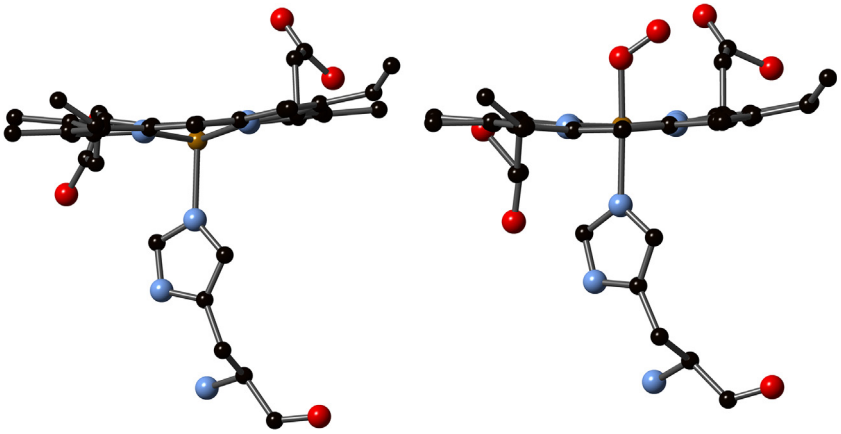

Fig. 3. The conformation of the heme core of human hemoglobin (Hb) as Hb (left) and oxyHb (right). Images generated from structures in references [39,40] (pdb codes 2 W72 and 2DN1, respectively).

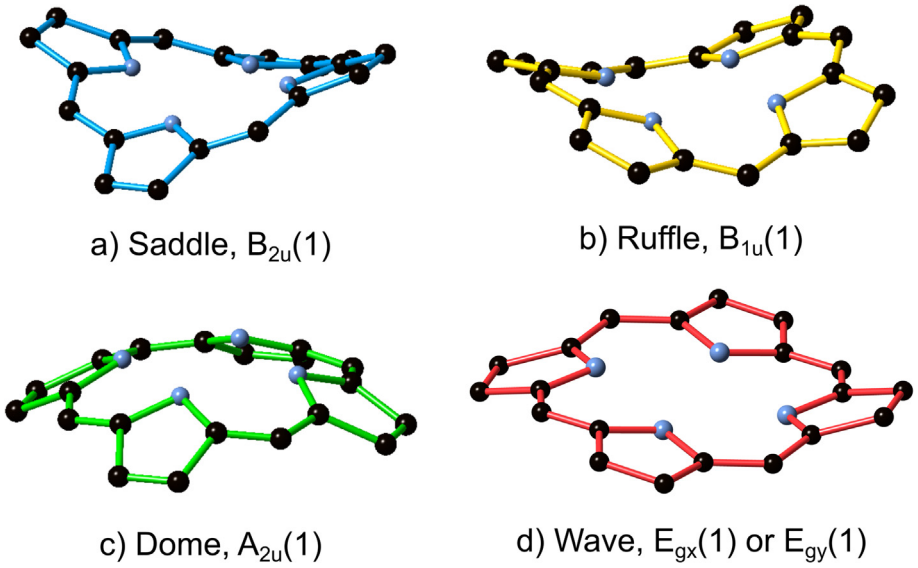

Fig. 4. The four principal modes of porphyrin 24-atom out-of-plane deformation – the saddle (B_{2u}, blue), ruffle (B_{1u}, yellow), dome (A_{2u}, green) and wave ($E_{g(x)}$ or $E_{g(y)}$, red).

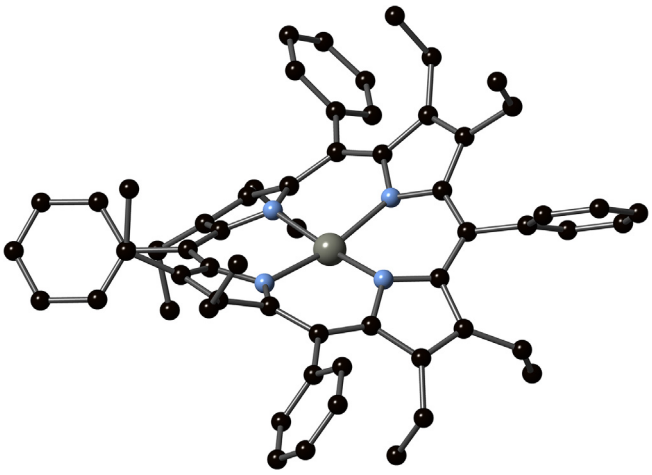

Fig. 5. View of the molecular structure in the crystal of (5,10,15,20-tetraphenyl-2,3,7,8,12,13,17,18-octaethylporphyrinato)zinc(II) methanol solvate [**4**•2MeOH, M = Zn(II)] demonstrating the saddle-shape out-of-plane distortion of the porphyrin core. Solvate and H-atoms are omitted from view. Image generated from CCDC No. 1185828, CSD code JICNIS [54].

distortion patterning, such as in the push-pull-type porphyrins [68].

Designing molecules with complimentary in-plane and out-of-plane structure allows for distorted macrocycles with ideal symmetry being substantially altered from the ideal D_{4h}. Examples of design of chiral porphyrins have used a saddle shape (B_{2u}) and differential substitution at the 5,15 and 10,20 position (B_{2g}) in either a porphyrin [64,65] or porphodimethene [70,71] to elicit a D_2-symmetric macrocyclic conformation. Chirality in supramolecular porphyrin complexes has been reviewed previously [72].

A strong bidirectional relationship between chemical substitution pattern and macrocyclic conformation can be used both to reliably design systems and to predict both structure and properties in systems for which direct structural information may not be available. Symmetry-by-design access to chiral porphyrin molecules – highly desirable compounds for use in catalysis and sensing – is somewhat stymied by lack of quantitative information of what effect a particular porphyrin substitution will have on the macrocycle shape, and to what magnitude. Individual crystal structures are susceptible to effects of crystalline solvate, intermolecular interactions and symmetry constraints of the solid state, which may affect the measured porphyrin shape. As such, one crystal structure is not necessarily representative of the same molecule's solution-phase symmetry.

This review describes an approach to assessing specific porphyrin distortional profiles, using crystallographic data mining [73] in combination with data pretreatment by Normal-coordinate Structural Decomposition (NSD) [29], to quantify distortion in reported porphyrin molecules in the CCDC CSD 2020.1 [74]. This method of assessing the complete literature for the design of molecules is a powerful tool to inform synthetic investigations, and necessary for the design of chiral porphyrins. Additionally, this dataset allows for crystallographers to fully contextualize the structure of novel molecules with reference to previously published structures. A program for assessment of novel crystal structures in relation to this data set is similarly described, and the set of tools which was used in this analysis is presented as well.

The method of deconvolution of structural effects in chromophores along symmetry-based normal coordinates is, we believe, an especially powerful tool for chemical understanding, as well as machine learning data pre-treatment. While this review is specifically restricted to porphyrin molecules, the potential applications of a wider application of the methods herein will be discussed later in Section 5.

The individual modes presented in Section 4 are intended to give an overview of the most accessible and prevalent distortional modes in porphyrin macrocycles, the substitution patterns required to attain them, and the factors affecting the extent of the mode as measured. Porphyrin compounds with similar substitution patterns cluster together in NSD terms, indicating that they adopt similar conformations. A list of these clusters, which often identify a bidirectional substitution pattern-conformational relationship, is provided in Tables 1 and 2, with justifications and discussion in Section 4. By no means an exhaustive list, this overview of the distortional profile invites others to attempt to break these soft rules, to furnish the literature with results outside the expected. In many cases, however, the mean structure of even

Table 1
The fitted structural deviation in NSD terms due to porphyrin core modifications.

Chemical substitution pattern	NSD modes affected (induced shape)	Value (NSD magnitude)	Standard deviation	Number of structures
Core modification				
M = 2H (free base), **6**, $R^{21,23}$ = H	$A_{1g}1$	0.164	0.027	709
	$B_{1g}2$	0.07	0.01	709
M = 4H (diacid), **6**, $R^{21\text{-}24}$ = H	$B_{2u}1$	3.082	0.885	82
	$B_{2u}2$	−0.703	0.135	82
mono and *cis*-dialkyl, **6**, R^{21} = C / $R^{21,22}$ = C	$B_{2u}1$	1.313	0.787	33
	$B_{2u}2$	0.375	0.223	33
trans-dialkyl, tri- and tetra-alkyl,	$B_{2u}1$	3.796	0.604	25
6, $R^{21,23}$ / $R^{21\text{-}23}$ /$R^{21\text{-}24}$ = C	$B_{2u}2$	−1.106	0.174	25
N-C-N Bridging motif, **6**, R^{21} = R^{22} = C	$E_{g(x)}1$ & $E_{g(y)}1$	0.530	0.131	9
		0.521	0.192	
N-N at pyrrole, **6**, R^{21} = N, $R^{22\text{-}24}$ = M or H	$B_{2u}1$	1.304	0.509,	21
	$B_{2u}2$	−0.435	0.091,	21
	$B_{1g}1$	0.157	0.094	22
5, M = Mg*	$A_{1g}1$	0.246	0.053	51
5, M = Mn*	$A_{1g}1$	0.077	0.102	167
5, M = Fe*	$A_{1g}1$	0.061	0.084	567
5, M = Co*	$A_{1g}1$	−0.040	0.096	144
5, M = Ni*	$A_{1g}1$	−0.104	0.136	314
5, M = Ni **	$A_{1g}1$	−0.371	0.210	528
	$B_{1u}1$	1.368	0.622	528
5, M = Cu*	$A_{1g}1$	0.032	0.071	140
5, M = Zn*	$A_{1g}1$	0.171	0.038	870
5, M = P, Si	$B_{1u}1$	1.909	0.989	36
	$A_{1g}1$	−0.358	0.312	36
Core bis-chelate i.e. **6**, R^{21} = R^{22} = MR^{23} = R^{24} = M′	$E_{g(x)}$ + $E_{g(y)}$*	1.022	0.271	12
Core bis-metallation, **6**, R^{21} = M, R^{23} = M′	$E_{g(x)}$ + $E_{g(y)}$*	0.57	0.369	99
5, M = Ln‡-L^2, L^2 = Phthalocyanine	$A_{2u}1$	0.795	0.087	66
	$A_{2u}2$	0.054	0.026	66
5, M = Ln‡-L^2, L^2 = Porphyrin	$A_{2u}1$	0.9	0.155	44
	$A_{2u}2$	−0.039	0.027	44
5, M = Ln‡-L^2, L^2 = non-pyrrolic	$A_{2u}1$	0.49	0.149	156
	$A_{2u}2$	−0.02	0.035	156
All Ln-porphyrin	$A_{2u}1$	0.615	0.243	274
	$A_{2u}2$	−0.005	0.046	274
	$A_{1g}1$	0.129	0.086	274

* Due to the significant effects of nonplanar distortion induced by peripheral substitution, only those porphyrins with Δ_{oop} < 1 are listed. ** Porphyrins with Δ_{oop} > 1. ‡ Ln = lanthanoid metal ions, Sc, Y + La:Lu and the larger metals Bi,Th,Pb,Zr,U,Hf in all oxidation states.

highly nonplanar porphyrins can be routinely predicted by knowing only the substitution pattern in an empirical manner. A guide to potentially overlooked pathways to chirality in porphyrins is presented. It is hoped that structural comparison in normal-coordinate terms becomes commonplace – a method is currently being developed by the authors to perform normal-coordinate structural decomposition on any collection of points, and visualizations of the same. This review is additionally intended to provide an example of the demonstrating quantitative structural analysis of immense numbers of crystal structures beyond the comparison of choice bond distances, angles or qualitative descriptors, and into comparative analysis of molecular conformation, even when molecules adopt a varied array of shape-combinations.

2. Methods

2.1. Normal-coordinate structural decomposition (NSD)

The quantification of structural effects of substitution is a natural evolution of the Normal-coordinate Structural Decomposition (NSD) method as originally developed by Shelnutt and coworkers [28,29,75]. NSD is the quantification of porphyrin atom positions by transform of cartesian atom positions as into magnitudes of concerted deviation of all atoms along symmetry-banded normal-coordinate modes, allowing these quantified distortions to be compared. These normal modes additionally carry symmetry information which directly allows for assessment of the symmetry of the porphyrin macrocycle (Fig. 6).

NSD relies on the generation of matrices which represent the calculated vibrational distortion modes of an idealized macrocycle, in this case (5,10,15,20-tetraphenylporphyrinato)copper(II) [2, M = Cu(II)] [76], which is used as a reference structure. Query atoms, such as those from a crystallographic structure solution, are then fitted to the reference structure *via* a least squares minimization [77], to remove the rotation and translational elements of the resultant matrix, and assigned to their corresponding atom in the reference structure [78]. The crystallographically determined atom positions are fitted, using a linear algebra least-squares method, to a linear combination of the optimized vibrational modes. In the implementation reported here, this fitting occurs at four levels of approximation: the minimum (lowest frequency mode per symmetric group) extended (lowest 2 modes) total (comparison of all calculated modes) and complete (square-root of the sum of squares of total modes) basis sets. Due to the modes being divided by symmetry elements, the in-plane and out-of-plane distortions can be treated independently.

A pair of overall distortion parameters (Δ_{oop} and Δ_{ip}) are assigned as the square root of the sum of squares of out-of-plane and in-plane distortions, respectively. The accrued error margins (δ_{oop} and δ_{ip}) are the sum of residual matrix elements – in the total case, this should equal zero, indicating a perfect fit to 66 parameters and no residual translational or rotational elements.

Table 2
The fitted structural deviation in NSD terms due to peripheral porphyrin modifications.

Periphery modification	NSD modes affected (induced shape)	Value (NSD magnitude)	Standard deviation	Number of structures
5, $R^{5,15} \neq H$, $R^{10,20} = H$, $R^{2,3,7,8,12,13,17,18} = H$	$B_{2g}1$	0.082	0.032	55
	$B_{2g}2$	0.026	0.023	55
6, $R^{5,15} \neq H$, $R^{10,20} = H$, $R^{2,3,7,8,12,13,17,18} = H$, R^{21},$R^{23} = H$	$B_{2g}1$	0.210	0.068	93
	$B_{2g}2$	0.110	0.033	93
5, $R^{5,15} \neq H$, $R^{10,20} = H$, $R^{2,3,7,8,12,13,17,18} \neq H$	$B_{2g}1$	0.270	0.090	35
	$B_{2g}2$	0.058	0.023	35
6, $R^{5,15} \neq H$, $R^{10,20} = H$, $R^{2,3,7,8,12,13,17,18} \neq H$, R^{21}, $R^{23} = H$	$B_{2g}1$	0.607	0.100	54
	$B_{2g}2$	0.136	0.035	54
5-monosubstituted, $R^{5} \neq H$, $R^{10,15,20} = H$	$B_{2g}1$	0.209	0.139	80
	$B_{2g}2$	0.055	0.039	80
5,10,15-trisubstituted, $R^{5,10,15} \neq H$, $R^{20} = H$	$B_{2g}1$	0.070	0.072	66
	$B_{2g}2$	0.015	0.026	66
5,15-Diexo-enylporphyrin	$B_{2g}1$	0.117	0.076	36
	$B_{2g}2$	0.007	0.249	36
	$A_{2u}1$	0.682	0.237	36
	$A_{2u}2$	−0.311	0.069	36
Picenoporphyrin	$B_{1g}1$	0.172	0.088	5
	$B_{1u}1$	0.057	0.044	5
trans-beta substitution **5**, $R^{2,3,12,13} \neq H$, $R^{7,8,17,18} = H$	$B_{1g}1$	0.135	0.092	78
	$E_{g(x)} + E_{g(y)}$[†]	0.214	0.161	78
Dodecasubstitution, $R^{2,3,5,7,8,10,12,13,15,17,18,20} \neq H$	$B_{2u}1$	2.701	1.136	379
	$B_{2u}2$	−0.322	0.248	379
Undecasubstitution, R^{2} or $R^{5} = H$	$B_{2u}1$	1.661	1.298	8
	$B_{2u}2$	−0.109	0.113	8
Decasubstitution Any two $R^{2\text{-}20} = H$	$B_{2u}1$	0.498	0.684	196
	$B_{2u}2$	−0.032	0.075	196
Supramolecular interaction with fullerene **5**·C_{60}	$A_{2u}1$	0.198	0.047	99
	$A_{2u}2$	−0.039	0.013	99

[†] Calculated as the sum of $E_{g(x)}$ and $E_{g(y)}$ modes, due to degeneracy of these modes.

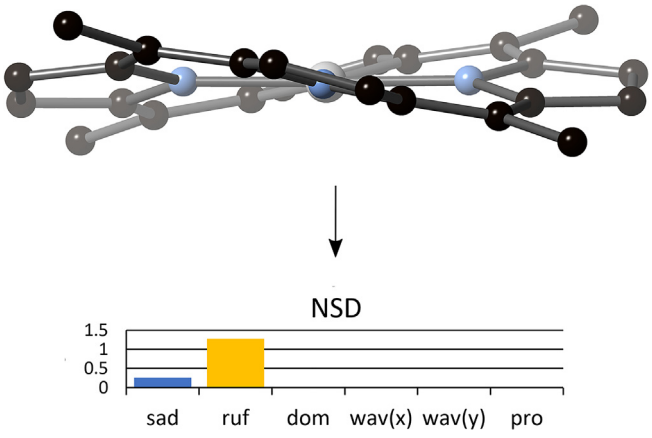

Fig. 6. The NSD program (Shelnutt, 1993) for individual molecular structure evaluation.

Despite the elegance of this method, the use of this technique has fallen out of favor as a characterization method, partly due to the unavailability of the original porphyrin-NSD program after the passing of Prof. Shelnutt in 2014 [79] and the complexity of the method discouraging reverse engineering. Additionally, interpreting this obfuscated data is difficult for non-specialists, especially without access to source code.

To revitalize NSD, we have written a new program which faithfully replicates and extends the original methodology in a modern programming language, Python 3.8, to assist with analysis of multiple structures, report generation and idealized structure generation. An interface to this program can be accessed online at https://www.sengegroup.eu/nsd, and the source code for this program is freely available from the authors as Supplementary Information (S.I. 6.5). A database of CCDC (version 2020.1) crystal structures in NSD terms is attached to this report as Supplementary Information (see S.I. 6.3). The introduction of a 'total' matrix report is the complete decomposition of coordinates into normal modes, without the uncertainty associated with approximation of the fewer degrees of freedom. This additional parameterization is intended to reduce uncertainty in structures derived retroactively from the NSD matrices, by tools provided in the program package (S.I. 6.5) for producing accurate coordinates of structure predictions. *Where the NSD program was originally designed for analysis of individual crystallographic determinations, this new program allows for the unattended, reliable analysis and comparison of large databases of structures.* This opens the door to cluster analysis, machine learning and a host of other methods of structural interrogation.

When querying a new crystal structure, the results of NSD analysis are presented in tabular and graphical form as indicated in Fig. 7. In the tables provided, each number is representative of the extent of distortion along the normal coordinate modes, which are presented in the S.I. sections S1 and S6.2. A graphical representation allows for immediate validation of results and structure assignment, to reduce results derived from incorrect structural fitting. Our intention is that this table and graphic could be included as SI information easily for papers which include porphyrin crystal structures, and that the further tables could assist the author in contextualizing structures and writing of the manuscript. The shift in research papers to have all research data available ('open data') in a concise manner is important when considering the new approach in publishing [80], with a machine-focus and data science (i.e. the quantitative approach) rightly taking precedence over the comparison of a handful of cherry-picked examples. Having data available in a format amenable to machine interrogation is an exceptional advantage, in the case for the Cambridge Crystallographic Data Centre Crystal Structure Database [74].

NSD result generated from file JICNIS at Mon Nov 9 14:03:27 2020
Summary of the NSD (in Å):

basis	Δ_{ip}	δ_{ip}	B_{2g}	B_{1g}	$E_u(x)$	$E_u(y)$	A_{1g}	A_{2g}
min.	0.39	0.05	-0.04	-0.01	-0.05	-0.01	-0.39	0.00
ext.	0.46	0.04	-0.04	-0.01	-0.05	-0.01	-0.39	0.00
			0.00	0.02	-0.04	-0.02	-0.24	0.04
total	0.59	0.00	-0.04	-0.01	-0.05	-0.01	-0.37	0.00
			0.00	0.02	-0.04	-0.02	-0.24	0.04
			0.01	0.01	-0.01	0.00	0.37	0.00
			0.00	0.00	0.02	0.01	0.00	0.00
			0.00	0.00	0.03	0.01	-0.03	0.00
			0.01	-0.01	0.01	0.00	-0.05	
					0.01	0.00		
					0.00	0.01		
					-0.01	0.00		
					-0.01	-0.01		
					-0.02	0.01		
comp.	0.59	0.00	0.04	0.03	0.08	0.03	0.58	0.04

basis	Δ_{oop}	δ_{oop}	B_{2u}	B_{1u}	A_{2u}	$E_g(x)$	$E_g(y)$	A_{1u}
min.	3.25	0.04	3.25	0.12	0.04	-0.04	-0.10	0.00
ext.	3.27	0.00	3.24	0.12	0.04	-0.04	-0.10	0.00
			-0.41	-0.02	0.03	0.00	-0.01	0.00
total	3.27	0.00	3.24	0.12	0.04	-0.04	-0.10	0.00
			-0.42	-0.02	0.03	0.00	-0.01	0.00
			-0.05	0.01	0.00	0.01	0.01	
						0.00	0.00	
						0.00	0.00	
comp.	3.27	0.00	3.27	0.12	0.05	0.04	0.11	0.00

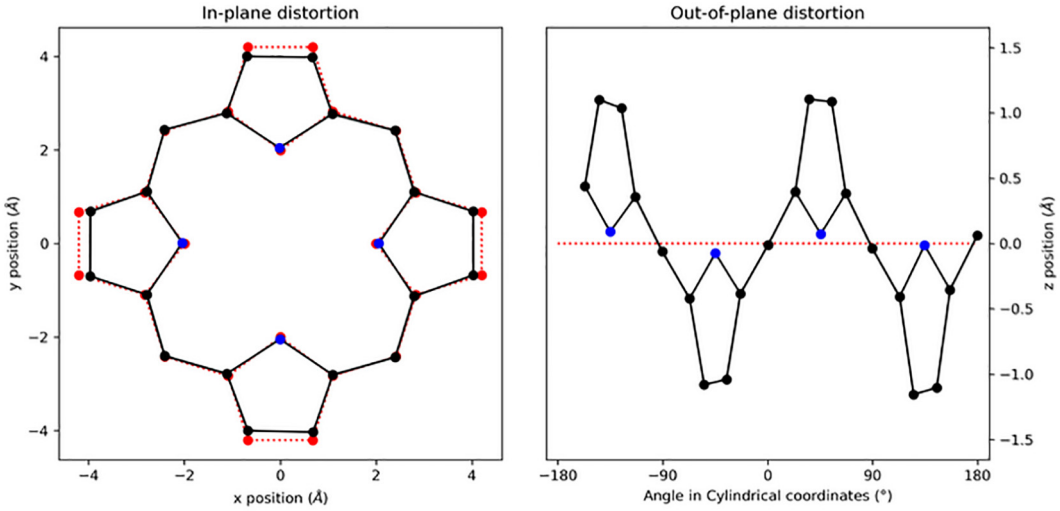

Fig. 7. The short-form results of an individual structure query to the new NSD web interface, for Zn(II)OETPP (Fig. 5); a longer form output is available, shown in Figs. S2.1-S2.4.

We believe strongly that a shift in scientific publishing toward availability of data, open presentation and interactive visualization as instructive and investigative tools are of paramount importance. To that end, we have provided the catalogued research data involved in the generation of the plots presented here, as a convenient Pandas DataFrame package. A convenient web portal for structure analysis and literature survey is available at https://www.sengegroup.eu/nsd. Additionally, interactive versions of the main distortional plots are provided online at https://www.sengegroup.eu/nsd_plots.html, intended to allow for researchers without computational specialization to gain a more complete understanding of the distortional landscape, or to investigate individual structures. A full toolkit, including the means to run the equivalent webserver is available as supplementary information (S.I. 6.5); with these tools, the entire database can be reconstructed from any large collection of porphyrin crystal structures.

This method was designed to be used in the routine reporting of crystal structures with a porphyrin core and has therefore been expanded from the original NSD methodology. A single page report suitable for S.I. (shown in Fig. 7) provides important characterization information; however, more information can be gleaned from the atom positions to assist with manuscript preparation. Tests applied to the NSD parameters can compare experimental values to clusters of structures based on chemical motifs, which are described in this paper, allowing for interrogation of specific chemical substitution-crystallographic structure relationships in small datasets. Additionally, this program reports symmetry point groups which can be conferred on the porphyrin subunit at predetermined levels and identifies the most similar structure by conformation in the CCDC and PDB databases, useful for structural comparison.

This contribution outlines the new NSD methodology and describes the most prominent distorted porphyrin types and relationships of chemical structure to crystal structure from analysis of the CSD data. A numerical basis for porphyrin shape can be described by the new web accessible NSD method; the statistical reduction of structural characteristics allows for novel structures to be contextualized simply in reference to all known structures. The method described here is published as a web-accessible program, allowing for researchers to submit .pdb format files of chemical or biogenic porphyrins and receive a thorough analysis of the porphyrin distortion (Fig. 7). This paper is intended to provide a referenceable guide of the porphyrin types, what they mean and how to design molecules to exploit these structural motifs.

2.2. Basic description of the NSD analysis program

A full description of how the program functions is provided in the comments of the attached source code. This NSD online program is written in python (version 3.8) with the libraries numpy [81], scipy [82], matplotlib [83], pandas [84], flask [85] and dependencies therein. The use of quaternion rotational minimization [77] and the Hungarian method [78] were keystone technologies in the fitting of an arbitrary structure to the model. In order to provide NSD results comparable to those in the literature currently, our program used distortion mode matrices provided by Jentzen *et al.* (S.I., S1 and S6.2) [29].

The NSD technique is based around a least-squares matrix reduction (implemented with numpy.linalg.lstsq) of porphyrin atom positions for which rotational and translational elements have been removed. The in-plane (x,y coordinates) and out-of-plane (z coordinates) structure can be treated separately, given the bifurcation of relevant symmetry modes. Each set of n vibrational modes (n = 6 (“min.”), 12 (“ext.”) or 21/45 (“comp.” & “total”), represented as a 24 × n (oop) or 48 × n (ip) mode coefficient matrix. Each of the analyses presented here are concerned with the output each of the modes separately, as the total matrix. A subsequent matrix was generated (total-f) which was sign-normalized in each case to the first mode of the symmetry group, intended to correct for the sign-agnostic orientation of the fitted macrocycle.

Database analysis was performed by identification and extraction of the porphyrinoid molecular substructure by CCDC-Mercury (using the CSD-Materials package) [74,86] or Protein Data Bank online interface [87,88] into a “.sd” file, and application of the above procedure. The calculated databases are included as Supporting Information, and available at www.kingsbury.id.au/data.

The testing for structural clustering behavior was based on identification of clusters of high distortion from plots of NSD parameters derived from database structures [89]. Structures were highlighted based on chemical substructures, from identifier lists extracted using CCDC-ConQuest [90]. Kernel Density Estimation (KDE, scipy.stats.gaussian_kde) [82,91] was used to visually identify bimodality in clusters. Two-dimensional bounds of identified structural distortion behavior were based on the ellipse defined by Pearson Chi-squared tensor at $\sigma < 2$, as indicated in the interactive versions of these plots (included as supplementary information, see S.I. S6.1). Cluster parameters are presented in S.I. Section S5.

3. Brief overview of the normal-coordinate analysis results

As stated above, NSD is a method of reductively and numerically describing the overall shape of a crystallographically identified porphyrin molecule using only a few parameters. The NSD method provides a numeric value of macrocyclic distortion, in Å, from the reference structure along each of the precomputed normal modes. As such, each of the data points in each of the plots in this review is an individual crystal structure with all extraneous structural minutiae stripped away, and each position on these axes represents a particular conformation of a reduced-symmetry macrocycle. Thus, the clustering of points due to an individual chemical moiety demonstrates mathematically that chemically similar molecules adopt the similar shapes, and with magnitudes approximated by a probability distribution.

The numerical value is, by convention, the sum movement of an individual pyrrole unit, or ¼ of the sum displacement of the macrocycle’s atoms along the normal coordinate vector. The precomputed modes are the vibrational normal modes, as calculated by Shelnutt [75], shown below to be approximations of the eigenvectors of the macrocyclic distortion in each symmetry operation class. Normal modes are depicted in the Supplementary information (S.I. Figs. S1.1 – S1.5) and tabulated in the attached source code, divided into those which occur in the plane of the ligand, and those resulting from out-of-plane movement, i.e. retention and rejection of σ_h symmetry. Normal modes are further divided into the symmetry classes attributable to the D_{4h} point group, the in-plane and out-of-plane distortions, respectively. The distortion modes, in general terms, align with specific chemical modifications of the porphyrin macrocycle which can be quantified and discussed.

The general form of a porphyrin macrocycle is presented in Fig. 1, with the R-groups representing the IUPAC-prescribed number of the porphyrin atom to which the group is attached. This numerical system is used throughout this paper. M represents either a metal center or another core moiety; for clarity, the groups $R^{21\text{-}24}$ are included in Fig. 1.

Certain types of core or peripheral modification can result in the presumed planar and aromatic porphyrin structure adopting a three-dimensional, nonplanar structure. Macrocycle atoms can, at extremes, deviate from the mean plane by more than 1 Å in

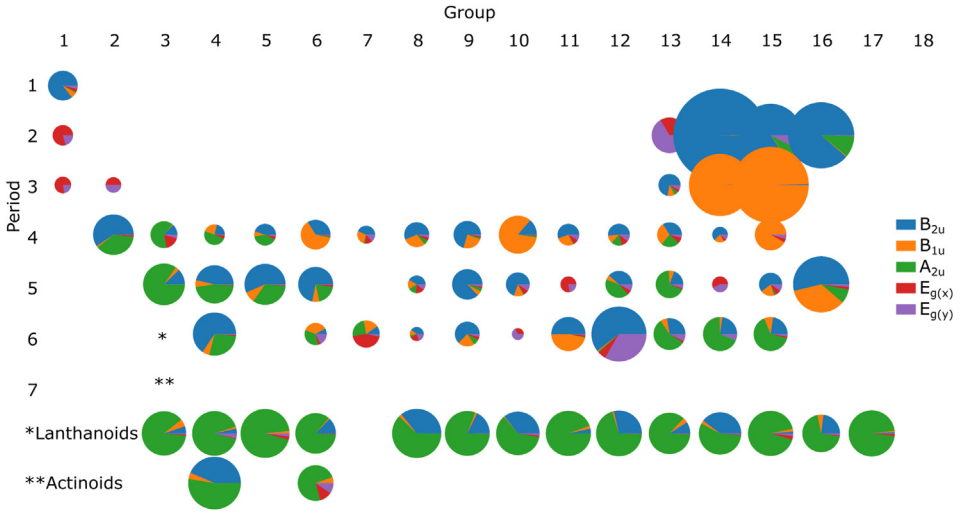

Fig. 8. A periodic table of porphyrin distortions, with log of the mean macrocyclic distortion represented as the size of each pie, divided into sections which represent the ratio of lowest frequency mode magnitude.

solution and the solid state [92,93] and even more at interfaces [94]. An altered conformation can induce a profound color change, and can lead to altered reactivity, especially at the C_m positions and with core protons. The methods and to produce varied types of non-planar porphyrins have become increasingly sophisticated due to the availability of techniques for formation of highly-substituted porphyrins and core and peripheral post-synthetic modifications, through organometallic and metal catalyzed techniques [46,47]. As a general overview we performed a statistical analysis of the CCDC entries with the most prominent substituent patterns. Table 1 summarizes the statistical result of the impact of core modifications on the macrocyclic conformation. Likewise, Table 2 comprises the statistical result of diverse peripheral substitution patterns. Both tables show that these structures are often predictable in both a qualitative and quantitative sense.

The out-of-plane modes which are most frequently encountered in crystal structures are correlated with the lowest frequency, or lowest energy vibrational modes; these are shown in Fig. 4. The *saddle* $B_{2u}(1)$ mode (Fig. 4a, blue) involves the tilting of individual pyrrole units in an up-down-up-down manner. The *ruffle* $B_{1u}(1)$ (Fig. 4b, yellow) involves the twisting of individual pyrrole units around the centroid-N axis, in a concertinaed +/−/+/− fashion. A *dome* $A_{2u}(1)$ (Fig. 4c, green) is the tilting of all pyrrole units in a concerted fashion towards one face, such as when chelating a large metal ion. A combination of the *wave* $E_{g(x)}$ and $E_{g(y)}$ 1st (Fig. 4d, red) and 2nd (Fig. S1.1) modes occurs as two dipyrrin halves tilt towards opposite faces, such that the individual pyrrole units tilt in in an up/up/down/down manner. In most of the other cases, other parameters have magnitude below the uncertainty of the crystallographic determination and have been traditionally ignored.

The formation of non-planar porphyrins can result from core or peripheral modification. A periodic table of porphyrin distortions is presented in Fig. 8 and shows the ratio and magnitude of the median distortion that results from binding core nitrogen atoms to specific atoms. Readily observed are that ruffling distortions result primarily from Ni(II) [95], but also from Si(IV) [96–98], P(V) [99–101], Cr(III) [102–104], As(V) [105,106] and Au(III) [107]. Introduction of lanthanoid or other large metal ions introduces a domed shape resulting from the sitting-atop type complex [108–112], and core-modification with pyrrole N-alkylation [22,113], or with the formation of an N-N [114] or N-O [115,116] bond initiates a dramatic increase in the B_{2u} (saddle) parameter. While this graphic generalizes multiple interactions (e.g., grouping free base and acid porphyrins together, as both involve N–H bonds) or differing bond character (e.g., oxidation states), this gives a general overview of the results of core modification.

Less dramatic, and often overlooked, are the in-plane distortions of the porphyrin macrocycle. The in-plane modifications of the macrocycle are regularly induced by core or peripheral substitution with a compatible symmetry to the distortional mode. An example of a core distortion is the $B_{1g}(2)$ mode, predominantly accessed by H_2 "free base" porphyrins. This molecular distortion can be rationalized as an angular change from the core protons altering the angle C_a-N-C_a in protonated (≈110°) vs. non-protonated (≈105°) pyrrole subunits.

The in-plane distortions which are most encountered in crystal structures are similarly correlated with the lowest frequency vibrational modes, as well as the totally symmetrical A_{1g} modes of isotropic expansion and contraction. The porphyrin can undergo isotropic expansion to accommodate a metal center or can be skewed by differential substitution around the macrocycle. Conceptually simplest might be the 5,15-disubstituted porphyrins which demonstrate a $C_5 \leftrightarrow C_{15}$ core elongation or meso-stretch across the core of the macrocycle – compare the equivalent $C_5 \cdots C_{15}$ at 6.88 Å in Zn(II)TPP [23], to 6.96 Å ($C_5 \leftrightarrow C_{15}$) vs 6.78 Å ($C_{10} \leftrightarrow C_{20}$) in (5,15-bis(4-tolyl)porphyrinato)zinc(II) [118]. In NSD terms, this stretch correlates with the first mode of B_{2g} symmetry and, when quantified, can be compared, as in Section 4.2 below.

In-plane distortion of the porphyrin moiety, while less dramatic, is essential to consider in the generation of chiral porphyrin cores. The A_{1u} mode, as the only chiral irreducible representation, is vanishingly rare, therefore multi-modal distortions are the best method of accessing chiral point-groups. The combination of one out-of-plane and a corresponding in-plane distortion has already been shown to form porphyrins with non-superimposable solid-state conformation [64] and used for chiral sensors [69–71]. In each case, the combination of a B_{2u} (saddle) and B_{2g} (meso-stretch) was used to achieve this chiral conformation. It is hoped by analyzing the data, other potential paths may be illuminated towards the generation of chiral porphyrins. The aim is that these compounds act as idealized receptors for photoactive chirality transfer, a method by which a chiral analyte will force the statistical adoption of a preferred chiral conformation [118]. This chiral enrichment can then be measured by absorption or fluorescence

methods, providing an easy and general method of chiral sensing based on porphyrin reporting units [69].

4. Analysis of porphyrin structures by cluster

The introduction of specific chemical motifs is, of course, generally known to induce structural distortion (e.g., with a 'H_4' core for saddle shape) in a qualitative sense. The redevelopment of the NSD algorithm, allowing for analysis of the large dataset of 6811 porphyrin molecules found in the CCDC CSD (2020.1) allow for a quantitative discussion on the effect of chemical substitution on structural distortion. Each porphyrin molecular core which has been structurally characterized can be reduced to a summation of symmetry-restricted vectors, and as such compared with other molecules; a similar NSD value represents a similar macrocyclic conformation.

In an ideal sense, derived values for multiple crystal structures can be analyzed as a collection of points, which cluster around a given value, and therefore a particular macrocyclic conformation [119,120]. Owing to similar molecules being responsive to similar forces controlling the macrocyclic conformation, one could expect that a similar shape would result. A cluster of NSD values deriving from a particular chemical modification shows a chemical structure/solid-state conformation relationship. When these are related to a probability function, this represents a probability distribution in 3D space, similar to a thermal ellipsoid. Demonstrated here is that certain types of porphyrin molecules show an NSD profile, and therefore solid-state conformation, consistent with other, similarly patterned molecules. Often, by introducing additional parameters which modulate the solid-state conformation, some individual chemical motifs will show a unique signature, allowing for structural verification. Of course, even identical porphyrin molecules vary slightly in solid state conformation, and therefore NSD profile, dependent on solvate or counter-ion, and we can now account for this in statistical terms.

The NSD parameters pertaining to individual chemical motifs can be isolated from one another given a sufficient sample size, forming clusters of similar structural conformation and chemical properties. That these clusters are so often tightly constrained indicates that the design regime employed for porphyrin molecules is similarly reliable, allowing for prediction of the structure of the identified porphyrin molecules by cluster analysis alone. For porphyrins of significant biological and materials science relevance, highly accurate structural data may not be available, and NSD analysis provides a useful tool for empirically grounded structure prediction and sanity-checking of results obtained through *ab initio* methods. We have taken such an approach in the past to elucidate the subtle changes in the bacterial photosynthetic reaction center [30] and light-harvesting complexes [121]. Additionally, the tools provided can yield structures for representative calculations.

These plots, representing the macrocyclic conformation, are possibly confusing at first inspection. It is important to remember that each point on each of the axes below represents simply a particular conformation of a macrocycle and a degree to which this occurs; that two points proximity in normal-coordinate space is equivalent to proximity of all atoms in real space, when the two structures are overlaid. Two compounds with the same parameters would necessarily be superimposable. In this sense, this can be described as a multi-atom equivalent of the common Ramachandran plot for macromolecular comparison [122,123].

The distinction of structural distortions into terms of the irreducible representations is due to the initial modes being derived from vibrational states. Similarly here, each irreducible representation is treated individually and these substitution effects, known to be orthogonal are implied to be similarly non-interfering, a necessary simplification which is only confounded by the presence of minor "compensatory" modes, discussed further in Section S4. This symmetry-stratification proves to be fortuitous in the quest for chiral porphyrins, as the necessary information for the providence of a point-group is provided directly in terms of the irreducible representations. Point groups are discussed further in Section 4.10. Indications are given for each cluster to the mean distortion attributable to the chemical structure, and covariance of in NSD terms. This can be thought of as a structural variance ellipsoid, relating many distinct structures to a probability attributable to the assigned substructure with the omission of small numbers of clear outliers. The structure codes related to each classification are listed in Section S3.

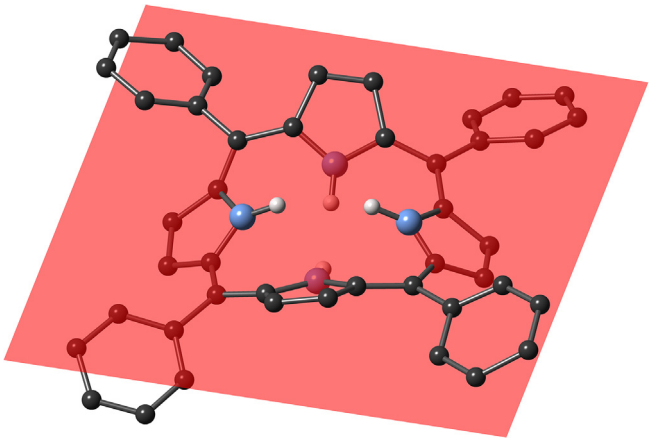

Fig. 9. The porphyrin saddle shape of $[H_4TPP]^{2+}$ in $[H_4TPP][Fe^{III}Cl_4](Cl)$, which shows 3.1 Å $B_{2u}(1)$ distortion magnitude. The mean plane of the molecule is presented in translucent red as a guide to the eye; C-bound H atoms have been omitted. Image generated from CCDC No. 1275452, CSD code TPPFEC [41].

In many of the NSD scatterplots demonstrated in this section, each parameter is plotted as the absolute value of the first mode, and the relative value of the second mode (e.g. $B_{2u}(2) \times$ sign $(B_{2u}(1))$ in each case, as these modes (with the exception of A_{1g}) are conformationally identical whether moving in the positive or negative direction, with sign depending on the orientation of the macrocycle with respect to the model compound. For this analysis, where each mode is treated independently, this is a valid mode of data pretreatment, however the relative sign of NSD modes in novel structures will be important in assigning a chiral conformation.

4.1. B_{2u}

The saddle shape, the first mode of B_{2u} distortional symmetry from porphyrin macrocycles is shown in Fig. 9. Characterized by the tilting of pyrrole units in an up-down-up-down manner, the saddle shape is commonly found in porphyrin diacid structures and in dodecasubstituted porphyrins. This conformation was the first structurally characterized, from pioneering work by Stone and Fleischer; distortion was introduced by acidification of the core to yield a 'H_4' porphyrin dication [41]. Similarly, nonplanarity has been classically introduced by steric conflict in macrocycles which are peripherally crowded, the so-called highly substituted porphyrins [46,124]. The series of dodecasubstituted porphyrins (i.e. all meso and beta positions non-H, e.g. **4**, OETPP, or **6** ($R^{2,3,7,8,12,13,17,18}$ = Br) OBrTPP) provides a clear structural type of porphyrin molecule which display some of the most egregious nonplanarity among porphyrins [54]. These effects have been demonstrated to act in concert [51].

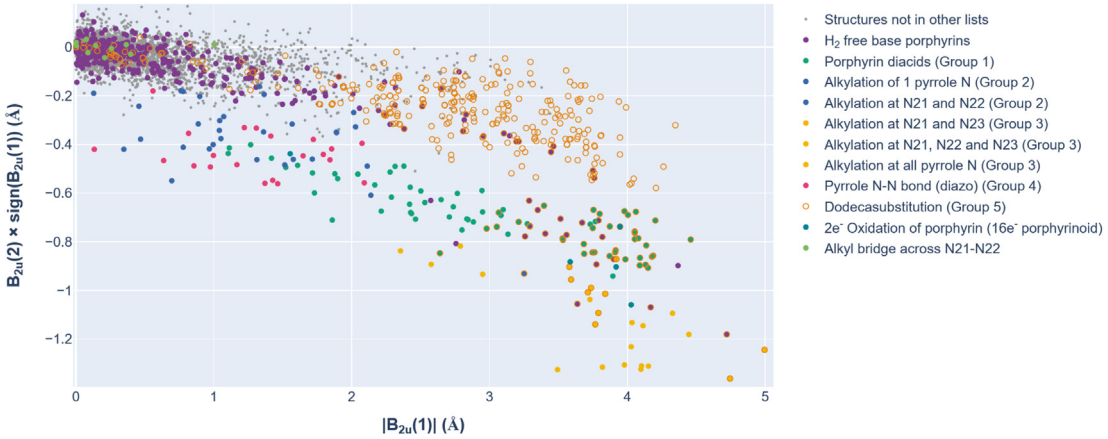

Fig. 10. Derived NSD parameters for core-modified and peripherally modified structures attributable to certain chemical motifs, along concerted vectors of the B_{2u} irreducible representation. The interactive version of this plot is available at https://www.sengegroup.eu/nsd_plots.html and in supplementary information [128].

The nonplanarity of macrocycles distorted in this fashion can be used for activation of the porphyrin core, allowing for interaction of core N–H donors with pocketed guests [57]. Distortion is similarly present in core-modified porphyrins in which steric conflicts are introduced between adjacent or opposite pyrrole nitrogen atoms; either though acidification to form H_4-porphyrin diacids, or by covalent formation of N–C and N–N bonds from the core. The absence of a metal center in the core, such as in free base porphyrins, is a secondary factor in modelling the extent of distortion of peripherally modified porphyrins. While not causing distortion along B_{2u}-symmetric modes alone, the free base porphyrins adopt a more distorted arrangement than their metallated counterparts, perhaps owing to additional flexibility.

4.1.1. Core modification

Fleischer and coworkers' pioneering work in the structural identification of porphyrin acids first demonstrated that porphyrins adopt a starkly nonplanar structure due to steric constraints. An alternating up-down-up-down orientation of pyrrole subunits around the porphyrin ring, a conformation which relates to the saddle mode presented in Fig. 9, is shared by the overwhelming majority of porphyrin diacids.

The B_{2u} NSD parameters for 'H_4' porphyrin diacids are shown in Fig. 10 in green filled circles. The core protonated porphyrins are a good example of a clear structural delineation; They are structurally distinct from most other porphyrins, and mostly exist in a single clearly defined cluster of conformations, with few outliers [64]. This conformational cluster is identified by the ellipsoid presented in Fig. 10, with the population of various conformations analogous to a thermal ellipsoid of an individual crystal structure. Fig. 10 similarly displays N–"C" [22,125,126] and N–"N" [114,127] – highly B_{2u}-distorted structures resulting from core modification. The measured saddling parameter broadly forms two clusters – those involving one N-alkyl, or two at N^{21} and N^{22} yield a mean sum distortion of 1.7 Å, and those with denser substitution patterns, at a mean of 4.7 Å. Structures with a N^{21}-C-N^{22} bridge show an E_g distortion pattern in place of this saddling and are discussed further in Section 4.6.

This "H_4 diacid" shape results from tilting of pyrrole units away from each other, and not towards a shared center, as would be the case in a metal complex or free base. These individual macrocyclic deformations have been fitted, with the relevant parameters shown in Table 1; an example of the two-dimensional calculation and the cluster-fitting result is shown in S4.2 and visualized in the interactive versions of these plots, available as supplementary information [128]. This same procedure of data fitting and gaussian approximation is followed for all other clusters mentioned in this review.

4.1.2. Peripheral modification

The primary method of introduction of large degrees of nonplanarity is the use of peri-interactions, e.g. in dodecasubstituted

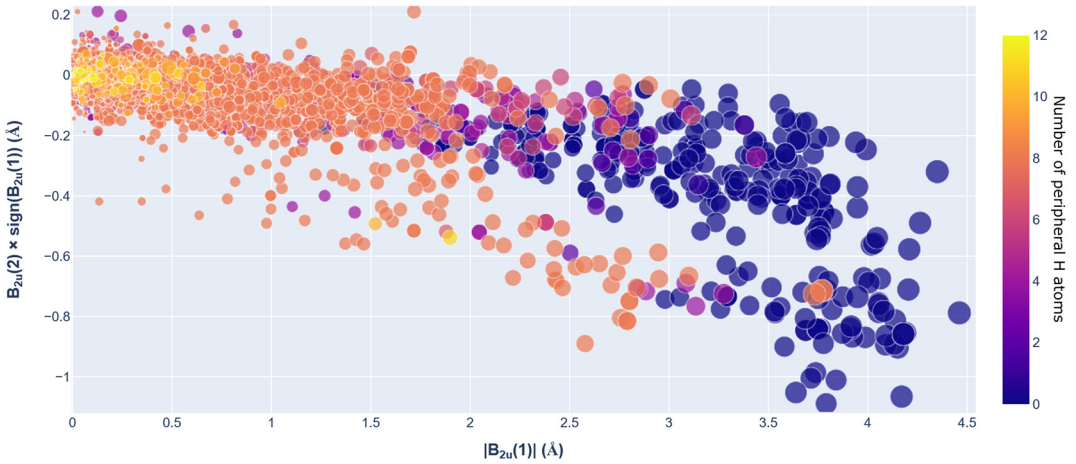

Fig. 11. The magnitude of B_{2u}(1) and (2) parameters, with marker color representing the number of H-atoms around the porphyrin periphery. As can be seen, a higher degree of non-H substitution leads to more distortion along the B_{2u} modes. H-number refers to number of C_b and C_m hydrogen atoms.

porphyrins – the formation of a porphyrin such as **4**, with all C_b and C_m positions filled by non-H atoms. The steric effects of dodecasubstitution to promote a saddle-distortion non-planarity are well known and, as seen in Fig. 11, is reflected in the correlation between B_{2u} parameter and fewer H-atoms around the porphyrin periphery [46,52].

The mean distortion along this mode for the 410 dodecasubstituted examples is 2.6(11) Å. The porphyrins with the greatest steric demand, such as 2,3,7,8,12,13,17,18-octaisopropyl-5,10,15,20-tetraphenylporphyrin (and oxidized derivatives), show the largest NSD parameters [129]. Some dodecasubstituted porphyrins, such as 2,3,5,7,8,10,12,13,15,17,18,20-dodecaphenylporphyrin (**5**, $R^{2,3,5,7,8,10,12,13,15,17,18,20}$ = Ph [130]) or 2,3,7,8,12,13,17,18-octaethyl-5,10,15,20-tetrakis(triisopropylsilylethynyl)porphyrin [131] are not necessarily saddle-shaped, though are often non-planar through ruffle or other distortion pathways; these porphyrins are discussed further in Sections 4.3 and 4.7. Some, such as 2,3,7,8,12,13,17,18-octa(phenylethynyl)-5,10,15,20-tetraphenylporphyrin (**5**, M = 2H, $R^{2,3,7,8,12,13,17,18}$ = C≡CPh, $R^{5,10,15,20}$ = Ph) are almost entirely planar due to lower steric demand [132]. Those structures with some β- and all four meso substituents show some structural distortion, generally less than the dodecasubstituted examples [52,133,134].

Those porphyrins with both a core and peripheral pattern (e.g., dodecasubstituted porphyrin diacids [93] or N-substituted derivatives [125]) promoting a saddle structure are among the most distorted structures, i.e. that multiple modifications to structure to engender specific distortion are additive. Comparing the dodecasubstituted 'H_4'-diacid subset ($|B_{2u}1|$ = 3.8(4) Å, n = 36) with the nondodeca 'H_4'-diacids ($|B_{2u}1|$ = 2.5(7) Å, n = 46) shows both that multiple strategies towards distortion can work synergistically, and that more intricate analyses of multiparametric distortional affect, such as those offered by machine learning studies, can narrow down specific structural magnitudes.

4.2. B_{2g}

B_{2g}, as distinct from the above B_{2u}, acts within the plane of the macrocycle. The B_{2g} distortion, or meso-stretch, is shown as in inset in Fig. 12(b & c), and can be imagined as the stretching of the C_5 and C_{15} containing axis of an otherwise symmetrical porphyrin core. Unsurprisingly, this distortion has been identified in compounds which have differential substitution at the meso positions of the porphyrin macrocycle. The simplest of these macrocycle types, such as 5,15-diphenylporphyrin (**6**, $R^{5,15}$ = Ph, $R^{10,20}$ = H, M = 2H), show an elongation of the substituted axis of around 0.3 Å. A scatterplot of the two predominant concerted coordinate vectors with B_{2g} representation are shown in Fig. 12. An interactive version (available at https://www.sengegroup.eu/nsd_plots.html) of this plot allows for the overlay of cluster information and interrogation of individual points.

The additional influence of the substitution at the C_b positions magnifies this distortional aspect, approximately tripling the observed distortion in the $B_{2g}(1)$ mode and adding positive distortion of around 0.12 Å along the $B_{2g}(2)$ mode; e.g., in 2,8,12,18-tetraethyl-3,7,13,17-tetramethyl-5,15-diphenylporphyrin [62]. The presence of a metal center at the core has a dampening effect, approximately halving the observed distortion when compared to free base porphyrins, irrespective of metal center. For example, (5,15-bis(*p*-tolyl)porphyrinato)zinc(II) [117] has a $B_{2u}(1)$ value of 0.11 Å vs 0.42 Å for the free base 5,15-diphenylporphyrin [64]. While these distortional magnitudes are significantly less than those for out-of-plane modes, preliminary investigations have indicated that a distortion of 0.2 Å is sufficient to induce measurable chiral effects in ideal systems. The few examples of compounds with a 5,15-dialkyl substitution pattern are among the most distorted [135].

Both meso mono- and trisubstituted porphyrins show generally less axial distortion than the 5,15-diarylporphyrin series, with

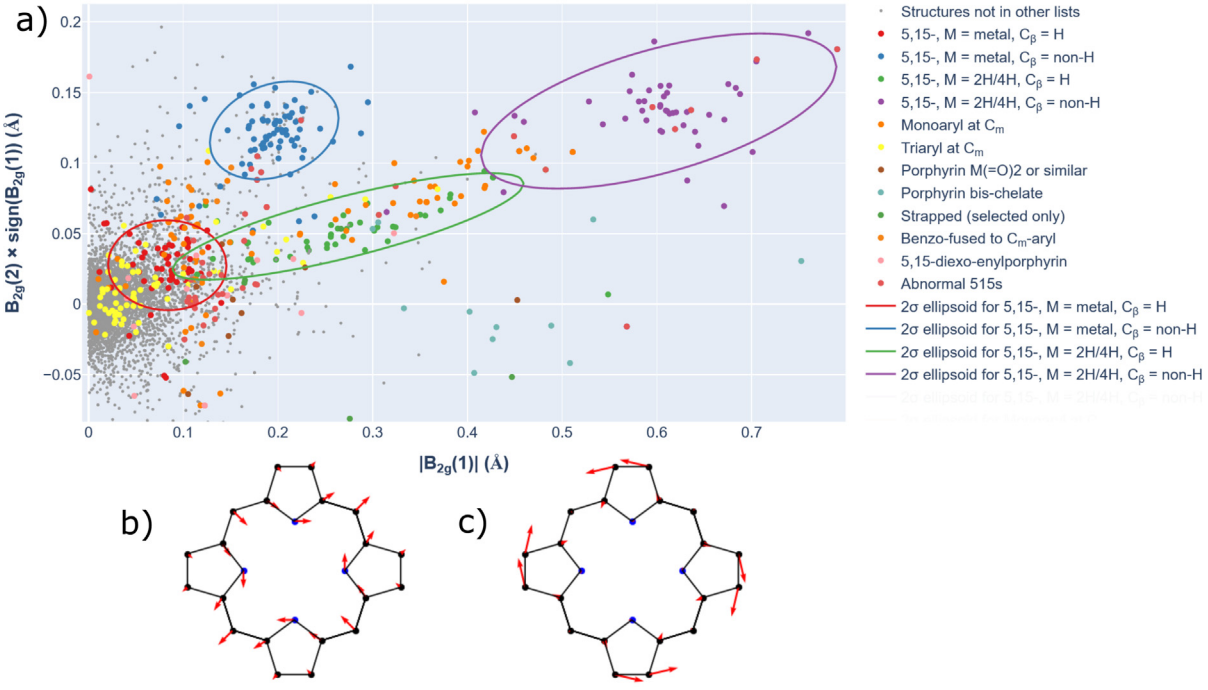

Fig. 12. The disposition of porphyrins along the B_{2g}-symmetric mode, with the 5,15-substitution pattern containing structures highlighted alongside other identified groups. The four most prominent groups are identified by ellipses, representing the 2(σ) boundary, indicated by the covariance matrix outlined in Section S4.3. Some examples fall outside of this plotting area, these are shown in the expanded interactive plot (S.I. 6.1) Parts b,c show the first and second fitted modes (x and y axes) of porphyrin B_{2g} distortion; arrows represent a 1.0 Å NSD parameter distortion along this mode.

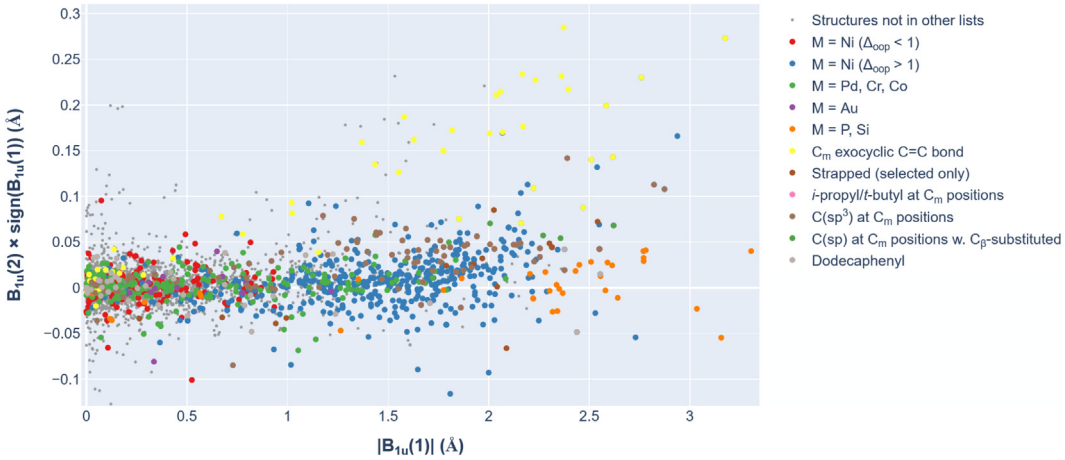

Fig. 13. Measured B_{1u}-symmetric distortion in the first and second modes of the macrocycle deformation.

mean values in $B_{2g}(1)$ of 0.21 and 0.07 Å, respectively. As with the 5,15- series, the most distorted are those examples with additional groups at C_b positions or alkyl substituents. Strong B_{2g} modes are also observed for compounds with a porphyrindione substructure, which has been used to elicit chirality previously [71]. The most strongly in-plane distorted structures are those structures which have a bis-chelating structure, with multiple boron or transition metal atoms bound to the core [157]. This bis-chelation can additionally result in significant and simultaneous $E_{g(x)}$ and $E_{g(y)}$ out-of-plane distortion; the B_{2g} distortion measured can be compared to the isotropic contraction 'shadow' which is concomitant with out-of-plane distortion, discussed further in S4.3.

4.3. B_{1u}

The primary distortion of B_{1u} symmetric representation, termed ruffling of the macrocycle, is shown in Figs. 1 and 2b), and involves a concertina-type folding of the porphyrin macrocycle, usually paired with an overall contraction. A scatterplot of the ruffling parameters observed for selected structural sublists is shown in Fig. 13. As hinted at in Fig. 5, and clearly seen here is the effect of nickel coordination; owing obviously to the large number of Ni(II)-porphyrin structures reported [95,136]. Traditionally, ruffling distortion has been correlated with the coordination of Ni (II) metal centers in the core – the small size of the Ni(II) ion draws pyrrole units closer to one another [26], as shown in A_{1g} Section 4.5. The induced steric demand placed upon the macrocycle by contraction is relieved by out-of-plane movement, as ruffling distortion [137–139]. As noted in Section 3, Ni(II) (ionic radius r_{ionic} = 0.83 Å)[177], Si(IV) (r_{ionic} = 0.54 Å), P(V) (r_{ionic} = 0.52 Å)], Cr(III) (0.755 Å), As(V) (0.60 Å) and Au(III) (0.99 Å) provide similar levels of ruffled distortion. Additionally, there are a significant number of Ni-containing porphyrins with little-to-no ruffling distortion. Ni(II) coordination is therefore not a sure-fire method of introduction of

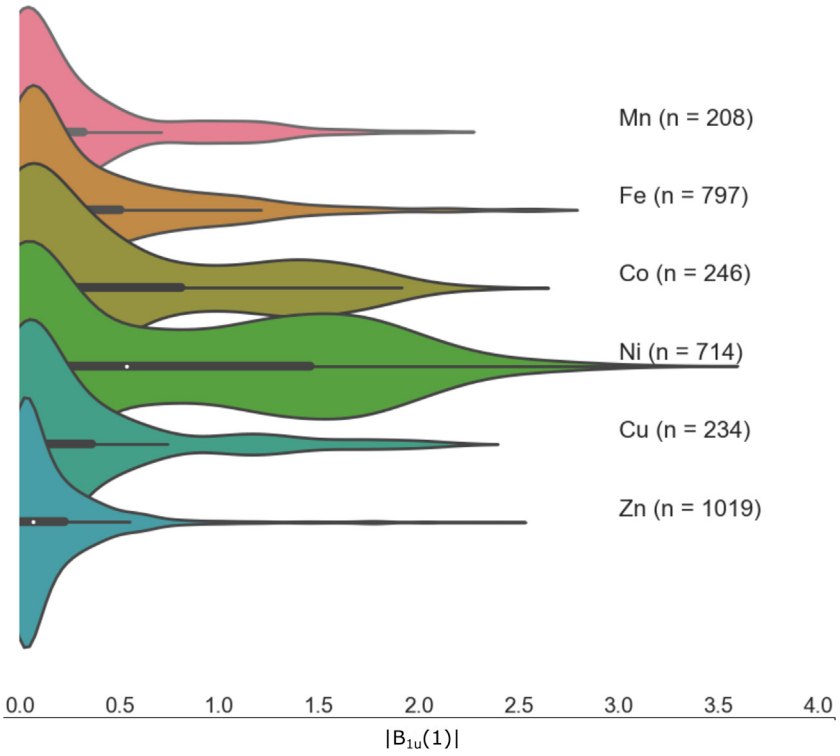

Fig. 14. A normalized violin plot of the relative B_{1u} distortion parameters of porphyrins coordinating late first-row d-block metals.

this modal distortion or dissymmetry [95,140]. As can be seen in Fig. 14, the ruffling distortion of Ni is still significant when compared to that observed for the metalloporphyrins with the other two most-reported metal centers; M = Fe and Zn.

Peripheral modification can similarly introduce a significant ruffled distortion, as is the case for the {5,10,15,20-tetrakis(*tert*-butyl)porphyrinato}zinc(II) [141]. A cluster of similarly distorted structures can be observed with R_{meso} = *t*Bu and *i*Pr, R_{meso} = alkyl generally, as well as those with R_{β} = non-H and R_m = C≡C—R′. Similarly, the formation of exocyclic C=C double bonds (in the 5,15-diexo-enyl porphyrins discussed in Section 4.6) induces a profound non-planar distortion, usually including a ruffling component. Generally, the success of each of these strategies is highly variable, with each class showing non-ruffled examples. More parameters may be required to ascertain the primary motivators for this specific distortional aspect.

4.4. B_{1g}

The B_{1g} mode of macrocyclic distortion involves the in-plane movement of two pyrrole units away from one another, and the remaining two towards one another. A plot of the magnitudes of this distortion is shown in Fig. 15. Each of the distortional modes is correlated with some difference in these pyrrole units. Free base porphyrins are distorted by the second B_{1g} mode, owing to protonation of N^{21} and N^{23} and concomitant change in angle of the C—N—C bond [142]. Compounds with substitution at the 2,3,12 and 13 positions ($R^{2,3,12,13} \neq H$, $R^{7,8,17,18} = H$) show more prominent distortion [143]. Similarly, those with alkylation of N^{21} and N^{23}, or those binding to different metals (N^{21}-M, N^{23}-M′) demonstrate very strong B_{1g} distortion in some cases [144]. Strapping from C_b positions and additional exocyclic ring fusion from C_b to C_m has many different effects due to a multitude of related but distinct examples, dependent on strap length and bond order [145]. These examples show both the largest magnitudes of distortion and no clear clustering behavior.

4.5. A_{1g}

The A_{1g} distortion of the macrocycle, obviously not indicative of any symmetry breaking movement of the porphyrin macrocycle, is nonetheless usually the largest in-plane distortional aspect observed for porphyrin molecules. Owing to the symmetric nature of this isotropic modality, A_{1g} distortion both acts as a compensatory mechanism for out of plane distortion (discussed further in S4) as well as a general measure of the symmetric impetus of individual metal chelation. An indicator of this is shown in Fig. 16, which relates the general isotropic size of planar (Δ_{oop} < 0.5 Å) porphyrins with the first-row transition metals.

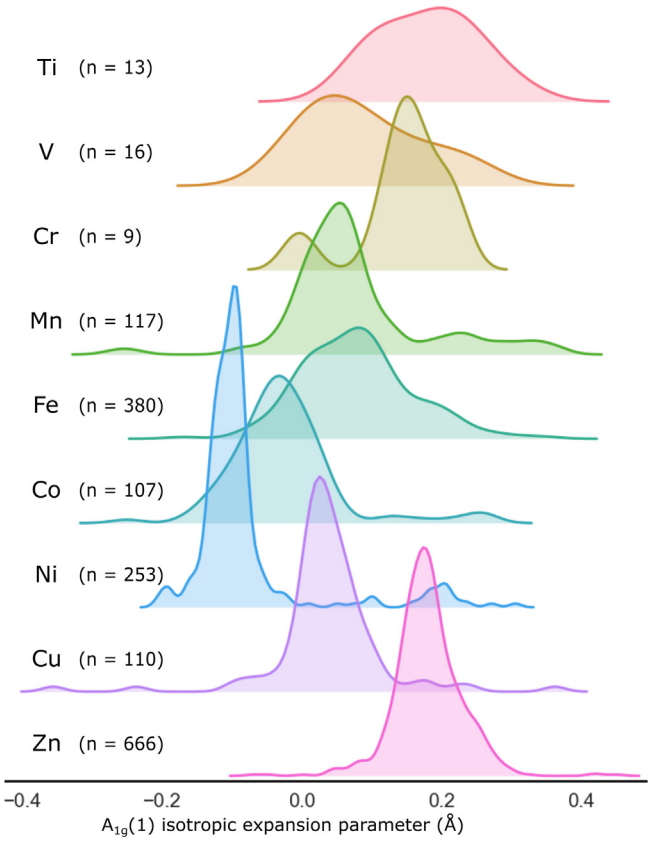

Fig. 16. Multiple-kernel density estimation plot relating first-row transition metal identity with the isotropic expansion and contraction of the metallated porphyrin. The kernel density estimation can be thought of as a continuous histogram; the normalized summation of Gaussian distributions using Silverman's distribution approximation [91].

As expected, the identity of the metal center at the core of the porphyrin dominates the contraction or expansion of planar porphyrins. Similarly, free base porphyrins have an isotropic expansive signature, as shown in Fig. 17.

This isotropic expansion and contraction is, however, far more widely variable when non-planar porphyrins are taken into

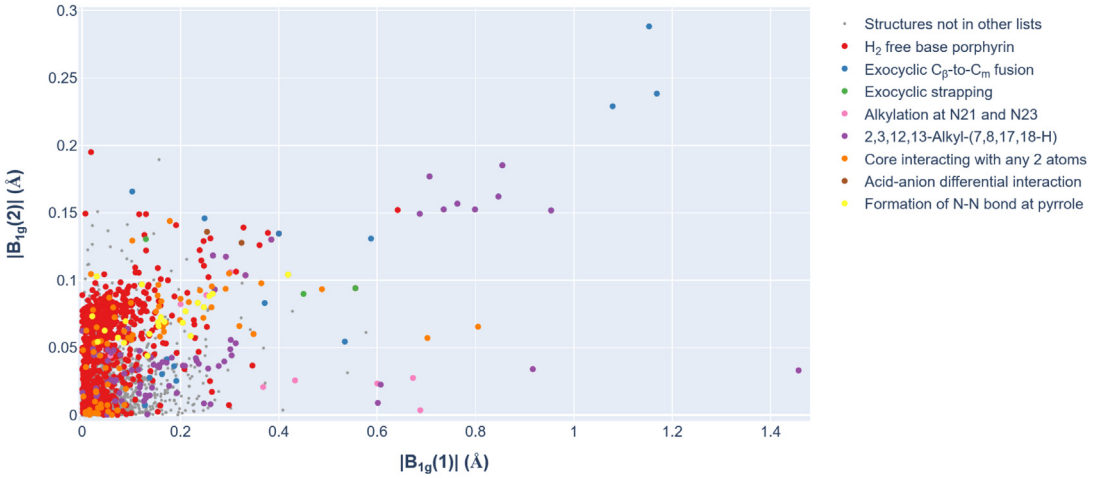

Fig. 15. The magnitudes of distortion along the B_{1g}-symmetry modes of porphyrin.

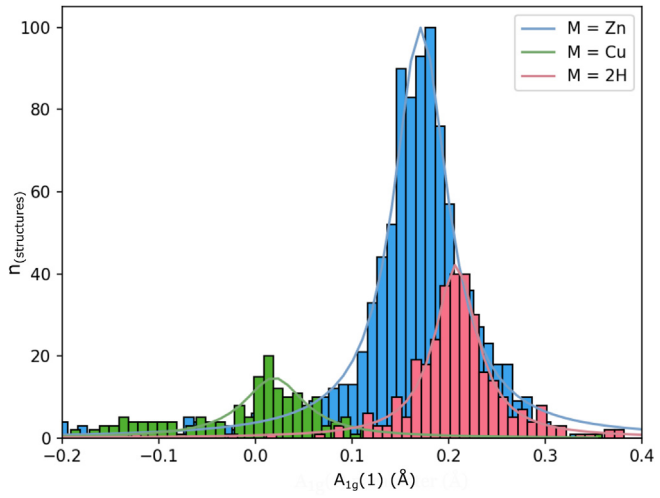

Fig. 17. A comparison of the histograms and fitted (least-squares) gaussian approximations of the isotropic expansion of core modified porphyrins with M = Zn (blue) M = Cu (green) and M = 2H (pink).

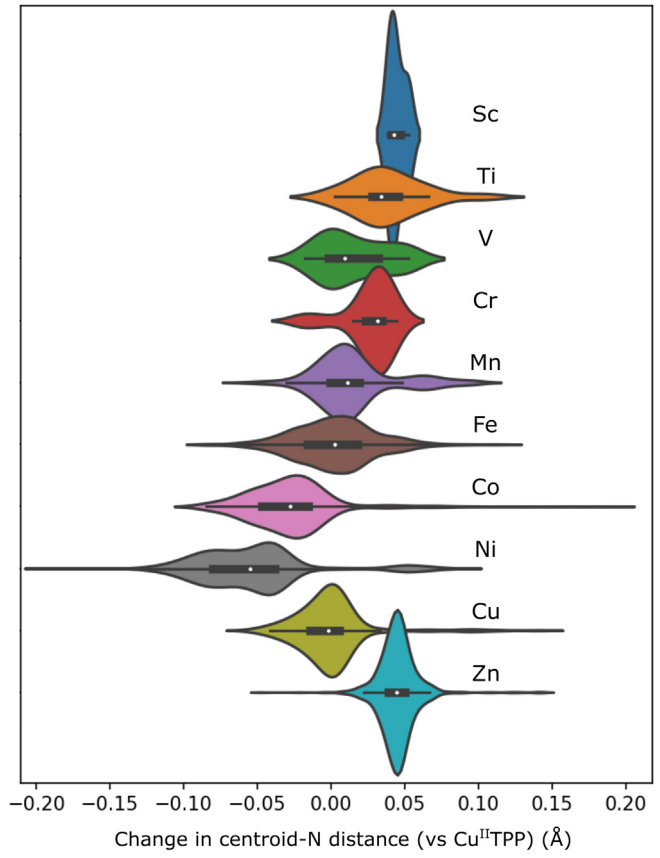

Fig. 18. Stacked violin plot of the N-displacement value with metal center identity, formed by multiplying the N-displacement matrix by the parameters (A_{1g}(1:6)). Additional nonsymmetric or out-of-plane distortion on N-atoms was not factored in.

account. A large out-of-plane distortion often results in contraction within the plane, just as a rod will cast a shorter shadow from an overhead lamp when raised at an angle [146]. The positioning of N-atoms should be a far more reliable indicator, and this can be provided directly from the NSD matrix by multiplying the N-displacement matrix ([0.200, 0.024, 0.375, 0.030, 0.204, 0.071]) by the A_{1g} distortional terms. The plot of isotropic expansion of the N-atoms when including nonplanar porphyrins is approximately equal to the distribution of the planar porphyrins, indicating that the M-N_4 substructure is seemingly altered only slightly by peripheral substitution patterns (Fig. 18).

4.6. A_{2u}

The A_{2u} mode represents movement of all four pyrrole units out of plane in concert – in the simplest representation, rotation towards the same face, directing the N-atoms to a point above the plane of the molecule. This dome-like formation can occur in several types of porphyrin, most simply in 'sit-atop' complexes of large metal centers. The magnitudes of A_{2u} distortion for several identified groups are shown in Fig. 19. The sit-atop complex is generally a structural feature of coordinated lanthanoid and similar metal centers with a large ionic radius and propensity for higher coordination numbers (i.e. ≥ 7).

The lanthanoid chelation at the core of the porphyrin offers three related shape-clusters, broadly dependent on the coordination environment of the metal center, but broadly similar between all lanthanoid (La:Yb) and related (Sc, Y, Th, Pb, Zr, U, Hf) large metal centers. Compounds with a single porphyrin chelating each metal centre are less distorted than those forming a sandwich-like bis-tetradentate structure, an example of which is shown in Fig. 20 [147]. A structural dimorphism exists within these sandwich compounds; clusters are broadly those of the form (OEP)Ln (Pc), with $A_{2u}(1) \times A_{2u}(2) < 0$, (upper (blue) ellipsoid in Fig. 19), and (TPP)Ln(Pc) sandwich compounds ($A_{2u}(1) \times A_{2u}(2) > 0$), with those of porphyrin-porphyrin dimer structures intermediate and intermingled with the two clusters. The parameters of the distortional motifs of lanthanoid compounds are plotted in Fig. 21, with this clustering behavior evident by kernel density estimation.

Another class of porphyrinoids with significant A_{2u} distortion are the porphyrindi-exo-enyl compounds, oxidized forms of the porphyrin moiety involving quinone and semiquinone moieties appended to the porphyrin ring. The porphyrindi-exo-enyl molecules discussed here are formally derivatives of 5,15-dioxoporphyrinogens and involve an exocyclic double bond from the 5- and 15-C_m positions of the porphyrin [148,149]. These molecules are important chemical intermediates in the formation of polycyclic porphyrin derivatives and are formally a $2e^-$ oxidation of the porphyrin core. This electronic modification induces a strong non-planar distortion, and molecules show vastly different absorption characteristics from porphyrins themselves. These compounds are strongly ruffle and-dome distorted simultaneously, as indicated in Section 4.3, in a similar manner to reduced porphyrin derivatives such as the porphodimethens ('calixdipyrrins') [150,151].

Fullerene-porphyrin assemblies are an example of a supramolecular interaction influencing the conformation of a porphyrin core and show a marked distortion towards non-planarity [152,153]. This conformational relief can be explained as the porphyrin conforming to the curved surface of the fullerene [154] – as such, this mode is seemingly absent in similar dyads with flat polycyclic aromatic hydrocarbons. Fullerenes introduce a modest distortion, of around 0.2 Å, along this conformational pathway. A typical example is shown in Fig. 22 [155].

4.7. $E_{g(x)}$ and $E_{g(y)}$

The porphyrin distortion modes $E_{g(x)}$ and $E_{g(y)}$ are activated by interaction of either an individual pyrrole, or two adjacent pyrrole units (i.e. N^{21} and N^{22}) with a metal complex which does not interact with N^{23} and N^{24}. In this way, the macrocycle is deformed along

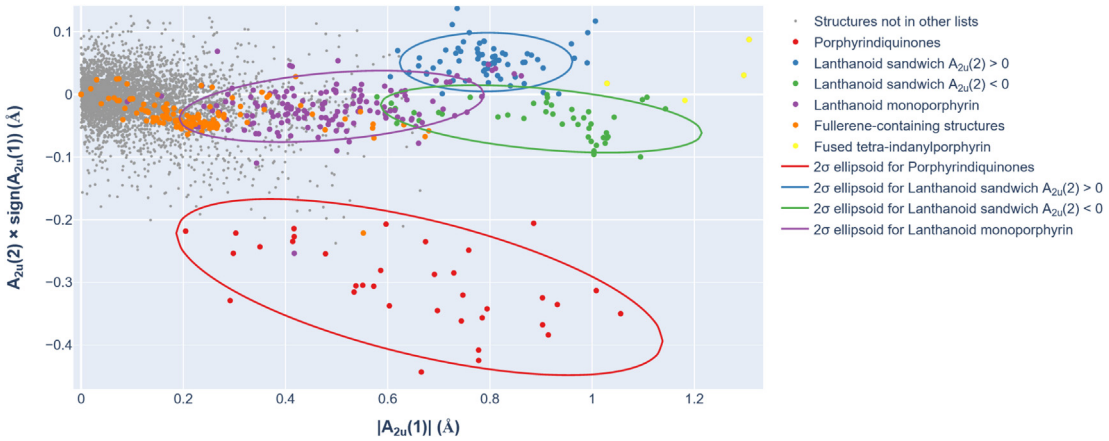

Fig. 19. The distortional profile of porphyrins in A_{2u} symmetry, with lanthanoid-coordinating porphyrins highlighted alongside porphyrindiquinones and those with a fullerene supramolecular interaction. Lanthanoid sandwich compounds are divided into two apparent clusters, with a positive and negative relative second A_{2u} parameter.

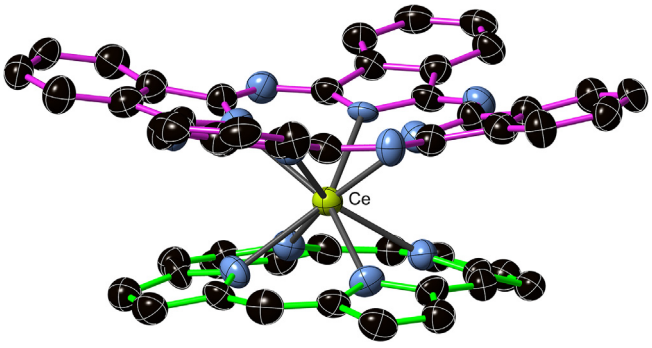

Fig. 20. A typical lanthanoid octaethylporphyrin-(na)phthalocyanine [Ce(IV)(**2**)(naphthalocyanine)] sandwich complex. Ethyl groups and hydrogen atoms on the porphyrin, and the extended terminal benzo-rings on the naphthalocyanine omitted. Image generated from CCDC No. 223659, CSD code ALIZOK [147].

one of the two equivalent wave-shaped modes shown in Fig. 4, or along a combination of the two modes, as shown in an example of a bis-Rh(I) porphyrin given in Fig. 23 [156]. The E_g distortional landscape is illustrated in Fig. 24.

The peripheral deformation strategies, such as differential and sterically demanding substitution at the 2,3,12,13-position of the porphyrin core (**5**, $R^{2,3,5,10,12,13,15,20} \neq H$, $R^{7,8,17,18} = H$) are not observed to be particularly effective at promoting a wave-shaped porphyrin outside of a few highly distorted examples, representing a poor graph-conformational bidirectional relationship. Core-modification strategies, particularly the formation of bis-chelates such as those with boron [157], or $(Rh^{I}(CO)_2)_2$ [156,158] as shown in Fig. 23 are effective, though only a few examples have been reported.

5. Discussion

5.1. Relation between NSD parameters and techniques for chirality conformer generation

As stated in the introduction, the formation, however transient, of a chiral porphyrin substructure is essential to the use of porphyrins as reporting units for chiral sensing. Different interactions with circularly polarized light, as expected by the energetic splitting of the a_{1u} orbital of Gouterman's model [50], offers a method to promote visible-light circular dichroism to measure chiral pollutants [72]. Additionally, the organocatalytic activity of a porphyrin unit [55], combined with a pre-arranged chirality induced by a chiral partner, may allow these units to function as chiral organocatalysts or photocatalysts without permanent chirality, reducing the cost and complexity of these transformative agents significantly. Each of these potential applications is reliant on the generally highly symmetrical porphyrin core becoming asymmetric with respect to the inversion, σ_h, $2\sigma_v$ and $2\sigma_v'$ symmetry operations in D_{4h}, and reducing to representation in D_4, C_4, D_2, C_2, or C_1 subgroups of D_{4h}.

Each individual mode of porphyrin distortion (except for the rarely present A_{1u}) results in a molecule with at least one mirror plane. The resultant symmetry groups from these distortions are tabulated in Table 3. Thus, the reliable introduction of chirality to a porphyrin relies on the simultaneous introduction of multiple distortional modes, such as those described in the previous section.

The combination of multiple modes resulting in the formation of a porphyrin with chiral point group is a process demonstrated previously [64,69–71,159–161] In each of these cases, the use of a B_{2g}-inducing substitution pattern (5,15-disubstitution) and a B_{2u}-inducing core modification (core acidification) resulted in molecules with D_2 symmetry. The introduction of two modes, as shown here, has a greater ability to introduce a wider range of symmetry groups. Table 4 shows the point group resulting from the introduction of two distortional modes simultaneously on a molecule of D_{4h} symmetry.

The demonstrated most-accessible chiral groups are therefore those in which a choice subset of the distortional modes are present, such as those enumerated as Type 1 to Type 4 below. Those which have an in-plane mode which is static and an out of plane mode which has some atropisomeric barrier to inversion provide the best chance of realizing chirality transfer, from an analyte, in a sensor capacity, or to a substrate for chiral catalysis [162].

As described above, the peripheral and core substitution strategies can work together for the generation of a chiral porphyrin core. A few examples of potential methods to engender chiral conformation, including the previously explored B_{2g} + B_{2u} combination, are enumerated in the following:

- Type 1: Saddle and C_m-stretch (B_{2g} + B_{2u}); e.g., saddled 5,15-disubstituted porphyrins [64,71,159].
- Type 2: Ruffle and N-stretching (B_{1g} + B_{1u}); e.g., ruffled *trans*-dibenzoporphyrins [163] or ruffled chlorins/bacteriochlorins and similar [164,165].
- Type 3: Domed and pyrrole rotation (A_{2g} + A_{2u}); e.g., lanthanoid tetraindolyl porphyrins [166].

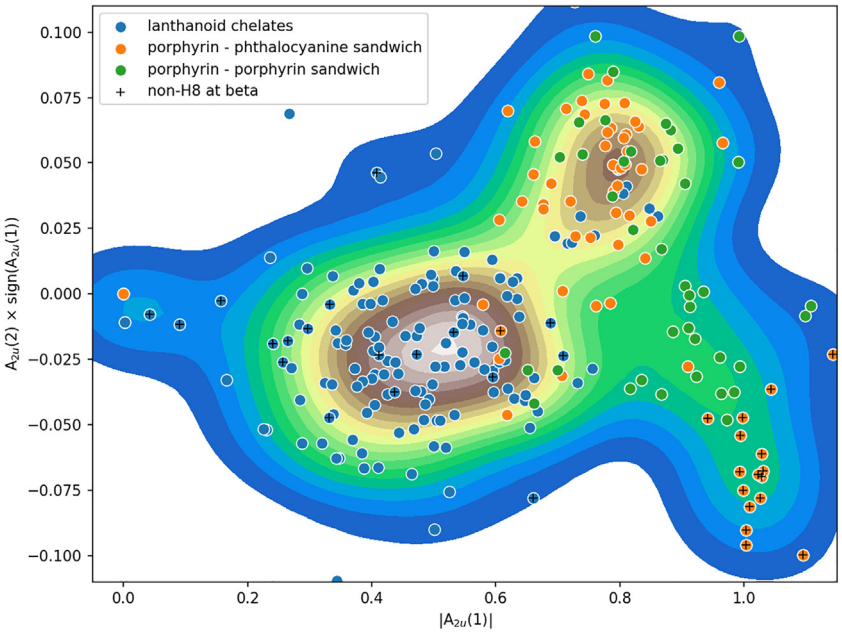

Fig. 21. Scatterplot of A_{2u} parameters of monoporphyrin-lanthanoid coordination compounds (blue) and bis-porphyrinoids (green and orange), overlaid on a kernel density estimation plot. The increased density and clustering of similar compounds indicates that there are three distinct conformational clusters for lanthanoid porphyrin coordination compounds.

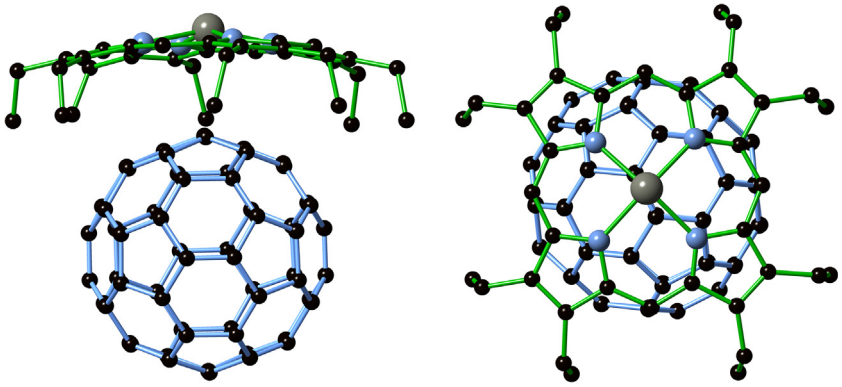

Fig. 22. Two views of a typical porphyrin-fullerene supramolecular complex ($ZnOEP{\cdot}C_{60}$) showing the dome-like distortion of the macrocycle. A DABCO co-ligand has been omitted from view. Image generated from CCDC No. 682233, CSD code COXMIM [155].

- Type 4: Domed, ruffled, and saddled porphyrins ($B_{2u} + B_{1u} + A_{2u}$), e.g., dodecasubstituted receptor porphyrins [59].

5.2. Some comments on the present analysis

Inherent in a database analysis of this type is that these data may hold an inherent bias, i.e. may not be representative samples of the total set of crystallizable molecules. Necessarily, the sample set for this analysis skews towards compounds which are synthetically achievable and crystallizable under standard conditions, and in the molecules which we and our colleagues choose to study and report. The effect of these multiple demands is impossible to ascertain, as no comparable total-set exists; however, by using statistical methods the influence of any individual data point is diminished. Necessarily, the focus in this review is on molecules which adopt different conformations and adopt certain specific structural 'types', i.e. a direct, 1:1 relationship between chemical structure and molecular conformation. Obviously, some nuance is eschewed here by design; a multiparametric modelling is a promising and computationally efficient manner of determining whether deeper relationships exist. Some non-isoelectronic derivatives of porphyrins, such as Lash's tropioporphyrin series [167] and the pyrrole-modified 'chlorins' obtained through Brückner's elegant 'breaking and mending strategy' [164,168] are not included in this analysis due to absence of a $C_{20}N_4$ porphyrin core; however, they offer a tantalizing route to symmetry-broken porphyrins. Similarly, the expansion of the above symmetry arguments to nonplanar phthalocyanines could lead to highly stable variants of the above [169].

The principal benefit of this publication is, we believe, that these extracted parameters provide a rapid means to contextualize asymmetry within porphyrins. Either by using the data set provided in Tables 1 and 2, or in the two-dimensional fits to the parameter space provided in Section S4, new structures can be contextualized as being within these named clusters, provided with a t-statistic, and shape can therefore be reduced to comparison of

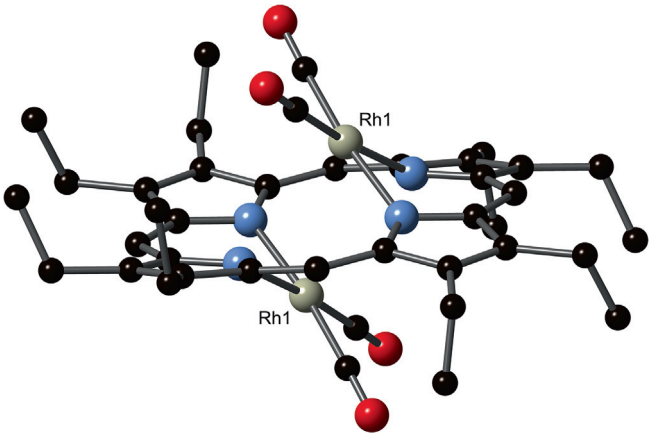

Fig. 23. View of the molecular structure in the crystal of $[Rh^{I}_{2}(\mathbf{2})(CO)_4)]$, showing strong E_g-symmetry distortion along the (x + y) direction, modelled as a combination of $E_{g(x)}$ and $E_{g(y)}$ distortions ($\Sigma E_{g(x)}$ = 0.62 Å, $\Sigma E_{g(y)}$ = 0.58 Å). Image generated from CCDC No. 1225717, CSC code OEPRHC10 [156].

a few numerical values. While the paper here is written entirely in reference to the small-molecule dataset, the full multiparametric dataset for protein porphyrins has been computed and is available from the authors [128]. A similar approach to using NSD parameters for protein data bank (PDB) analysis has been published recently, based on the lowest frequency modes [170,171]. The NSD program reported here can be used to extract values for novel protein crystal structure coordinates of isolated porphyrin ligands to compare with the values in the PyDISH database. Furthermore, clustering of the porphyrin distortions with multiple normal modes per symmetry operation, similar to the analysis performed here, could be potentially useful to parameterize allosteric effects across the large protein data set.

6. Conclusions

The structural variance attributable to a simple, versatile chemical unit, the porphyrin, is demonstrated to be both empirically predictable and strongly indicative of chemical substitution pattern, oxidation state and exocyclic linkages. The comparison between multiple structures and the demonstration of consistent motifs indicates that the design regime is persistent and should extrapolate to systems where atomic crystallographic data cannot be gained, in enzymes, on surfaces, and in solution. The stark conformational differences resulting from substitution patterning embolden the prospect and potentials of designing a range of porphyrins with responsive aromatic chirality.

The clear demonstration of a link between normal-coordinate structure and chemical modification is one which can be extrapolated in a similar manner to other chemical systems. The clear indication of a single predominant mode of distortion per symmetry argument leads one to believe that the precomputed tables, while computationally efficient, are an unnecessary computational component of NSD analysis. On this basis, we are developing an empirical system to perform symmetry-gated normal-coordinate analysis on arbitrary chemical systems, particularly for chromophore subunits. We believe new tools will allow similar normal-coordinate based analyses to be performed with ease, and for this type of quantitative structure comparison to become commonplace in crystallography. The link between the available structural data and the symmetry underpinning could perhaps inform similar distortion-seeking chemical modification and designed synthesis with other simple aromatic structures, such as the BODIPY series [172–174]. Normal-coordinate studies are an elegant method of quantifying and contextualizing measured dissymmetric structural distortion and could be equally applied to other structure-property relationships.

A clear structural delineation and definable structural behavior, as evidenced by close clusters of similarly patterned molecules, could be rationalized for the A_{1g}, B_{1u}, B_{2u}, B_{2g} and A_{2u} parameter sets. The muddied and variable behavior in context of each of the other parameters under study is implicative of a multiparametric relationship between chemical structure and molecular conformation. This form of large conformational comparison analysis is not common, and as such, the simplest version was intended to be presented here.

We have demonstrated that a molecular frame, from analysis of a very large number of examples, has perhaps many fewer degrees of freedom than would be imagined, implying that a rational parameter-reduction can be made on symmetric grounds. This type of dimension reduction analysis could assist algorithms in the assignment of correct structure from low-data diffraction techniques; for example, by reducing the parameter space. The parameter reduction and clear line from molecular conformation

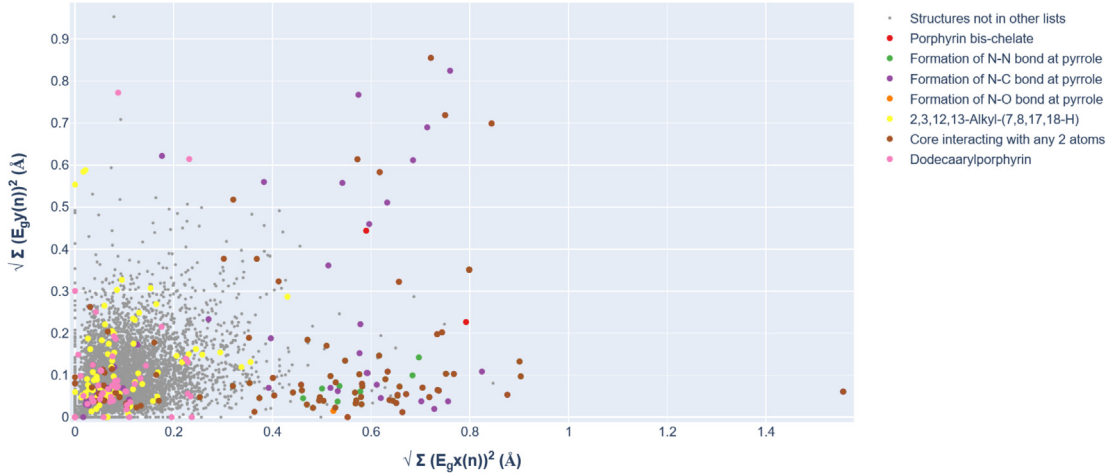

Fig. 24. A scatterplot of the 'comp' NSD values, or sum distortion of porphyrins along the E_g distortional modes, in both the x- and y-oriented forms. An interactive version of this plot is available at https://www.sengegroup.eu/nsd_plots.html and in supplementary information [128].

Table 3
Symmetry resulting from singular distortions applied to any molecule of D_{4h} symmetry, e.g., a porphyrin.

Distortion Mode	B_{2g}	B_{1g}	$E_{u(x)}$	$E_{u(y)}$	A_{1g}	A_{2g}	B_{2u}	B_{1u}	A_{2u}	$E_{g(x)}$	$E_{g(y)}$	A_{1u}
Resulting point group	D_{2h}	D_{2h}	C_{2v}	C_{2v}	D_{4h}	C_{4h}	D_{2d}	D_{2d}	C_{4v}	C_{2h}	C_{2h}	D_4

Table 4
Symmetry resulting from two distortions applied to a porphyrin. *The E-modes, when both present are considered to have equal magnitude here, e.g., $|E_{g(x)}(n)| = |E_{g(y)}(n)|$ such that the resulting mode also has E_g or E_u symmetry.

	B_{2g}	B_{1g}	$E_{u(x)}$	$E_{u(y)}$	A_{1g}	A_{2g}	B_{2u}	B_{1u}	A_{2u}	$E_{g(x)}$	$E_{g(y)}$	A_{1u}
B_{2g}	D_{2h}	C_{2h}	C_s	C_s	D_{2h}	C_{2h}	D_2	C_{2v}	C_{2v}	C_i	C_i	D_2
B_{1g}	C_{2h}	D_{2h}	C_{2v}	C_{2v}	D_{2h}	C_{2h}	C_{2v}	D_2	C_{2v}	C_{2h}	C_{2h}	D_2
$E_{u(x)}$	C_s	C_{2v}	C_{2v}	C_{2h}*	C_{2v}	C_s	C_s	C_2	C_s	C_2	C_s	C_2
$E_{u(y)}$	C_s	C_{2v}	C_{2h}*	C_{2v}	C_{2v}	C_s	C_s	C_2	C_2	C_s	C_2	C_2
A_{1g}	D_{2h}	D_{2h}	C_{2v}	C_{2v}	D_{4h}	C_{4h}	D_{2d}	D_{2d}	C_{4v}	C_{2h}	C_{2h}	D_4
A_{2g}	C_{2h}	C_{2h}	C_2	C_s	C_{4h}	C_{4h}	S_4	S_4	C_4	C_i	C_i	C_4
B_{2u}	D_2	C_{5v}	C_s	C_s	D_{2d}	S_4	D_{2d}	S_4	C_{2v}	C_s	C_s	D_2
B_{1u}	C_{2v}	D_2	C_2	C_2	D_{2d}	S_4	S_4	D_{2d}	C_{2v}	C_2	C_2	D_2
A_{2u}	C_{2v}	C_{2v}	C_s	C_s	C_{4v}	C_4	C_{2v}	C_{2v}	C_{4v}	C_s	C_s	C_4
$E_{g(x)}$	C_i	C_{2h}	C_2	C_s	C_{2h}	C_i	C_s	C_2	C_s	C_{2h}	C_{2v}*	C_2
$E_{g(y)}$	C_i	C_{2h}	C_s	C_2	C_{2h}	C_i	C_s	C_2	C_s	C_{2v}*	C_{2h}	C_2
A_{1u}	D_2	D_2	C_2	C_2	D_4	C_4	D_2	D_2	C_4	C_2	C_2	D_4

parameter, through measurement, to photophysical properties, combined with the wealth of data available for these analyses, indicates that this form of computational analysis is ideally suited to machine learning [175,176]. Additionally, due to the reduced parameter space there exists the potential for using spectral data for structure assignment, not merely structural correlation, an enticing prospect should these relationships be parameterized [177]. Finally, this analysis provides a clear rationale and pathway to maximizing the efficiency of various types of chiral-aromatic porphyrins, a subset of designed materials with a bright future in sensing and catalysis.

Declaration of Competing Interest

The authors declare that they have no known competing financial interests or personal relationships that could have appeared to influence the work reported in this paper.

Acknowledgements

This work has received funding from the European Union's Horizon 2020 research and innovation program under the under the FET Open grant agreement No. 828779 (project INITIO) and was supported by Science Foundation Ireland (IvP 13/IA/1894). This work was prepared with the support of the Technical University of Munich – Institute for Advanced Study through a Hans Fischer Senior Fellowship.

Appendix A. Supplementary data

Supplementary data to this article can be found online at https://doi.org/10.1016/j.ccr.2020.213760.

References

[1] A.R. Battersby, Tetrapyrroles: the pigments of life, Nat. Prod. Rep. 17 (2000) 507–526, https://doi.org/10.1039/b002635m.
[2] E. Sitte, M.O. Senge, The red color of life transformed – synthetic advances and emerging applications of protoporphyrin IX in chemical biology, European J. Org. Chem. 2020 (2020) 3171–3191, https://doi.org/10.1002/ejoc.202000074.
[3] M.O. Senge, A.A. Ryan, K.A. Letchford, S.A. MacGowan, T. Mielke, Chlorophylls, symmetry, chirality, and photosynthesis, Symmetry 6 (2014) 781–843, https://doi.org/10.3390/sym6030781.
[4] T.L. Poulos, Heme enzyme structure and function, Chem. Rev. 114 (2014) 3919–3962, https://doi.org/10.1021/cr400415k.
[5] B. Grimm, R.J. Porra, W. Rüdiger, H. Scheer, Chlorophylls and Bacteriochlorophylls: Biochemistry, Biophysics Functions and Applications, Springer, Dordrecht, 2007.
[6] S. Yoshikawa, A. Shimada, Reaction mechanism of cytochrome c oxidase, Chem. Rev. 115 (2015) 1936–1989, https://doi.org/10.1021/cr500266a.
[7] J.S. Lindsey, Synthetic routes to meso-patterned porphyrins, Acc. Chem. Res. 43 (2010) 300–311, https://doi.org/10.1021/ar900212t.
[8] M.O. Senge, Stirring the porphyrin alphabet soup—functionalization reactions for porphyrins, Chem. Commun. 47 (2011) 1943–1960, https://doi.org/10.1039/c0cc03984e.
[9] M.O. Senge, N.N. Sergeeva, K.J. Hale, Classic Highlights in Porphyrin and Porphyrinoid Total Synthesis and Biosynthesis, Chem. Soc. Rev. (2021), accepted for publication..
[10] K. Norvaiša, M. Kielmann, M.O. Senge, Porphyrins as colorimetric and photometric biosensors in modern bioanalytical systems, ChemBioChem 21 (2020) 1–16, https://doi.org/10.1002/cbic.202000067.
[11] M. Ethirajan, Y. Chen, P. Joshi, R.K. Pandey, The role of porphyrin chemistry in tumor imaging and photodynamic therapy, Chem. Soc. Rev. 40 (2011) 340–362, https://doi.org/10.1039/b915149b.
[12] A. Wiehe, J.M. O'Brien, M.O. Senge, Trends and targets in antiviral phototherapy, Photochem. Photobiol. Sci. 18 (2019) 2565–2612, https://doi.org/10.1039/c9 pp00211a.
[13] R. Costa e Silva, L.O. da Silva, A. de Andrade Bartolomeu, T.J. Brocksom, K.T. de Oliveira, Recent applications of porphyrins as photocatalysts in organic synthesis: batch and continuous flow approaches, Beilstein J. Org. Chem. 16 (2020) 917–955, https://doi.org/10.3762/bjoc.16.83.
[14] M. Urbani, M. Grätzel, M.K. Nazeeruddin, T. Torres, Meso-substituted porphyrins for dye-sensitized solar cells, Chem. Rev. 114 (2014) 12330–12396, https://doi.org/10.1021/cr5001964.
[15] A.A. Ryan, M.O. Senge, How green is green chemistry? Chlorophylls as a bioresource from biorefineries and their commercial potential in medicine and photovoltaics, Photochem. Photobiol. Sci. 14 (2015) 638–660, https://doi.org/10.1039/c4 pp00435c.
[16] L. Arnold, K. Müllen, Modifying the porphyrin core - a chemist's jigsaw, J. Porphyrins Phthalocyanines 15 (2011) 757–779, https://doi.org/10.1142/S1088424611003720.
[17] M. Yedukondalu, M. Ravikanth, Core-modified porphyrin based assemblies, Coord. Chem. Rev. 255 (2011) 547–573, https://doi.org/10.1016/j.ccr.2010.10.039.
[18] P.J. Chmielewski, L. Latos-Grazyński, Core modified porphyrins - a macrocyclic platform for organometallic chemistry, Coord. Chem. Rev. 249 (2005) 2510–2533, https://doi.org/10.1016/j.ccr.2005.05.015.
[19] A.D. Adler, F.R. Longo, F. Kampas, J. Kim, On the preparation of metalloporphyrins, J. Inorg. Nucl. Chem. 32 (1970) 2443–2445, https://doi.org/10.1016/0022-1902(70)80535-8.
[20] S. Hiroto, Y. Miyake, H. Shinokubo, Synthesis and functionalization of porphyrins through organometallic methodologies, Chem. Rev. 117 (2017) 2910–3043, https://doi.org/10.1021/acs.chemrev.6b00427.
[21] M.O. Senge, Nucleophilic substitution as a tool for the synthesis of unsymmetrical porphyrins, Acc. Chem. Res. 38 (2005) 733–743, https://doi.org/10.1021/ar0500012.

[22] M. Roucan, K.J. Flanagan, J. O'Brien, M.O. Senge, Nonplanar porphyrins by N-substitution: a neglected pathway, European J. Org. Chem. 2018 (2018) 6432–6446, https://doi.org/10.1002/ejoc.201800960.
[23] M.P. Byrn, C.J. Curtis, Y. Hsiou, S.I. Khan, P.A. Sawin, S.K. Tendick, C.E. Strouse, A. Terzis, Porphyrin sponges: conservation of host structure in over 200 porphyrin-based lattice clathrates, J. Am. Chem. Soc. 115 (1993) 9480–9497, https://doi.org/10.1021/ja00074a013.
[24] A. Ozarowski, H.M. Lee, A.L. Balch, Crystal environments probed by EPR spectroscopy. Variations in the EPR spectra of CoII(octaethylporphyrin) doped in crystalline diamagnetic hosts and a reassessment of the electronic structure of four-coordinate cobalt(II), J. Am. Chem. Soc. 125 (2003) 12606–12614, https://doi.org/10.1021/ja030221f.
[25] A. Maclean, G. Foran, B. Kennedy, P. Turner, T. Hambley, Structural characterization of Nickel(II) tetraphenylporphyrin, Aust. J. Chem. 49 (1996) 1273–1278, https://doi.org/10.1071/CH9961273.
[26] J.L. Hoard, Stereochemistry of hemes and other metalloporphyrins, Science 174 (1971) 1295–1302, https://doi.org/10.1126/science.174.4016.1295.
[27] M.O. Senge, S.A. MacGowan, J.M. O'Brien, Conformational control of cofactors in nature-the influence of protein-induced macrocycle distortion on the biological function of tetrapyrroles, Chem. Commun. 51 (2015) 17031–17063, https://doi.org/10.1039/c5cc06254c.
[28] W. Jentzen, J.G. Ma, J.A. Shelnutt, Conservation of the conformation of the porphyrin macrocycle in hemoproteins, Biophys. J. 74 (1998) 753–763, https://doi.org/10.1016/S0006-3495(98)74000-7.
[29] W. Jentzen, X.Z. Song, J.A. Shelnutt, Structural characterization of synthetic and protein-bound porphyrins in terms of the lowest-frequency normal coordinates of the macrocycle, J. Phys. Chem. B 101 (1997) 1684–1699, https://doi.org/10.1021/jp963142h.
[30] S.A. MacGowan, M.O. Senge, Conformational control of cofactors in nature-functional tetrapyrrole conformations in the photosynthetic reaction centers of purple bacteria, Chem. Commun. 47 (2011) 11621–11623, https://doi.org/10.1039/c1cc14686f.
[31] S.A. MacGowan, M.O. Senge, Computational quantification of the physicochemical effects of heme distortion: redox control in the reaction center cytochrome subunit of blastochloris viridis, Inorg. Chem. 52 (2013) 1228–1237, https://doi.org/10.1021/ic301530t.
[32] A. Forman, M.W. Renner, E. Fujita, K.M. Barkigia, M.C.W. Evans, K.M. Smith, J. Fajer, ESR and ENDOR probes of skeletal conformations implications for conformations and orientations of chlorophylls in vivo, Isr. J. Chem. 29 (1989) 57–64, https://doi.org/10.1002/ijch.198900009.
[33] M.O. Senge, New trends in photobiology. The conformational flexibility of tetrapyrroles - current model studies and photobiological relevance, J. Photochem. Photobiol. B Biol. 16 (1992) 3–36, https://doi.org/10.1016/1011-1344(92)85150-S.
[34] J.A. Shelnutt, X.Z. Song, J.G. Ma, S.L. Jia, W. Jentzen, C.J. Medforth, Nonplanar porphyrins and their significance in proteins, Chem. Soc. Rev. 27 (1998) 31–41, https://doi.org/10.1039/a827031z.
[35] D.R. Davydov, J.R. Halpert, Allosteric P450 mechanisms: multiple binding sites, multiple conformers of both?, Expert Opin. Drug Metab. Toxicol. 4 (2008) 1523–1535, https://doi.org/10.1517/17425250802500028.
[36] C.M. Woods, C. Fernandez, K.L. Kunze, W.M. Atkins, Allosteric activation of cytochrome P450 3A4 by α-naphthoflavone: branch point regulation revealed by isotope dilution analysis, Biochemistry 50 (2011) 10041–10051, https://doi.org/10.1021/bi2013454.
[37] Y. Yuan, M.F. Tam, V. Simplaceanu, C. Ho, New look at hemoglobin allostery, Chem. Rev. 115 (2015) 1702–1724, https://doi.org/10.1021/cr500495x.
[38] M.F. Perutz, Stereochemistry of cooperative effects in haemoglobin: haem-haem interaction and the problem of allostery, Nature 228 (1970) 726–734, https://doi.org/10.1038/228726a0.
[39] S.Y. Park, T. Yokoyama, N. Shibayama, Y. Shiro, J.R.H. Tame, 1.25 Å resolution crystal structures of human haemoglobin in the oxy, deoxy and carbonmonoxy forms, J. Mol. Biol. 360 (2006) 690–701, https://doi.org/10.1016/j.jmb.2006.05.036.
[40] C. Savino, A.E. Miele, F. Draghi, K.A. Johnson, G. Sciara, M. Brunori, B. Vallone, Pattern of cavities in globins: the case of human hemoglobin, Biopolymers 91 (2009) 1097–1107, https://doi.org/10.1002/bip.21201.
[41] A. Stone, E.B. Fleischer, The molecular and crystal structure of porphyrin diacids, J. Am. Chem. Soc. 90 (1968) 2735–2748, https://doi.org/10.1021/ja01013a001.
[42] W.R. Scheidt, Y.J. Lee, Recent advances in the stereochemistry of metallotetrapyrroles. In: J.W. Buchler (Ed.), Metal Complexes with Tetrapyrrole Ligands I. Structure and Bonding, vol 64. Springer, Berlin, Heidelberg (1987). DOI:10.1007/BFb0036789. ISBN 978-3-540-17531-5..
[43] W.R. Scheldt, Trends in metalloporphyrin stereochemistry, Acc. Chem. Res. 10 (1977) 339–345, https://doi.org/10.1021/ar50117a005.
[44] C.J. Medforth, M.O. Senge, K.M. Smith, L.D. Sparks, J.A. Shelnutt, Nonplanar distortion modes for highly substituted porphyrins, J. Am. Chem. Soc. 114 (1992) 9859–9869, https://doi.org/10.1021/ja00051a019.
[45] B. Röder, M. Büchner, I. Rückmann, M.O. Senge, Correlation of photophysical parameters with macrocycle distortion in porphyrins with graded degree of saddle distortion, Photochem. Photobiol. Sci. 9 (2010) 1152–1158, https://doi.org/10.1039/c0 pp00107d.
[46] M.O. Senge, Highly Substituted Porphyrins, in: K.M. Kadish, K.M. Smith, R. Guilard (Eds.), The Porphyrin Handbook, Vol. 1, Academic Press, San Diego, pp. 239–347..
[47] M.O. Senge, Exercises in molecular gymnastics - bending, stretching and twisting porphyrins, Chem. Commun. (2006) 243–256, https://doi.org/10.1039/b511389j.
[48] C.M. Drain, S. Gentemann, J.A. Roberts, N.Y. Nelson, C.J. Medforth, S. Jia, M.C. Simpson, K.M. Smith, J. Fajer, J.A. Shelnutt, D. Holten, Picosecond to microsecond photodynamics of a nonplanar nickel porphyrin: Solvent dielectric and temperature effects, J. Am. Chem. Soc. 120 (1998) 3781–3791, https://doi.org/10.1021/ja974101h.
[49] R.E. Haddad, S. Gazeau, J. Pécaut, J.C. Marchon, C.J. Medforth, J.A. Shelnutt, Origin of the red shifts in the optical absorption bands of nonplanar tetraalkylporphyrins, J. Am. Chem. Soc. 125 (2003) 1253–1268, https://doi.org/10.1021/ja0280933.
[50] M. Gouterman, Spectra of Porphyrins, J. Mol. Spectrosc. 6 (1961) 138–163, https://doi.org/10.1016/0022-2852(61)90236-3.
[51] M.O. Senge, T.P. Forsyth, L.T. Nguyen, K.M. Smith, Sterically strained porphyrins—influence of core protonation and peripheral substitution on the conformation of tetra-meso-, octa-β-, and dodecasubstituted porphyrin dications, Angew. Chem., Int. Ed. Engl. 33 (1995) 2485–2487, https://doi.org/10.1002/anie.199424851.
[52] W.W. Kalisch, M.O. Senge, Synthesis and structural characterization of nonplanar tetraphenylporphyrins with graded degree of β-ethyl substitution, Tetrahedron Lett. 37 (1996) 1183–1186, https://doi.org/10.1016/0040-4039(95)02405-0.
[53] S. Gentemann, C.J. Medforth, T.P. Forsyth, D.J. Nurco, K.M. Smith, J. Fajer, D. Holten, Photophysical properties of conformationally distorted metal-free porphyrins. Investigation into the deactivation mechanisms of the lowest excited singlet state, J. Am. Chem. Soc. 116 (1994) 7363–7368, https://doi.org/10.1021/ja00095a046.
[54] K.M. Barkigia, J. Fajer, M.W. Renner, M. Dolores Berber, C.J. Medforth, K.M. Smith, Nonplanar porphyrins. X-ray structures of (2,3,7,8,12,13,17,18-octaethyl-and-octamethyl-5,10,15,20-tetraphenylporphinato)zinc(II), J. Am. Chem. Soc. 112 (1990) 8851–8857, https://doi.org/10.1021/ja00180a029.
[55] M. Roucan, M. Kielmann, S.J. Connon, S.S.R. Bernhard, M.O. Senge, Conformational control of nonplanar free base porphyrins: towards bifunctional catalysts of tunable basicity, Chem. Commun. 54 (2017) 26–29, https://doi.org/10.1039/c7cc08099a.
[56] W. Suzuki, H. Kotani, T. Ishizuka, T. Kojima, A mechanistic dichotomy in two-electron reduction of dioxygen catalyzed by N, N'-dimethylated porphyrin isomers, Chem. - A Eur. J. 26 (2020) 10480–10486, https://doi.org/10.1002/chem.202000942.
[57] M. Kielmann, M.O. Senge, Molecular engineering of free-base porphyrins as ligands—the N–H···X binding motif in tetrapyrroles, Angew. Chemie - Int. Ed. 58 (2019) 418–441, https://doi.org/10.1002/anie.201806281.
[58] M. Kielmann, C. Prior, M.O. Senge, Porphyrins in troubled times: a spotlight on porphyrins and their metal complexes for explosives testing and CBRN defense, New J. Chem. 42 (2018) 7529–7550, https://doi.org/10.1039/c7nj04679k.
[59] K. Norvaiša, K.J. Flanagan, D. Gibbons, M.O. Senge, Conformational re-engineering of porphyrins as receptors with switchable N–H···X-type binding modes, Angew. Chem. Int. Ed. 58 (2019) 16553–16557, https://doi.org/10.1002/anie.201907929.
[60] K. Norvaiša, J.E. O'Brien, D.J. Gibbons, M.O. Senge, Elucidating atropisomerism in nonplanar porphyrins with tunable supramolecular complexes, Chem. Eur. J. (2020), https://doi.org/10.1002/chem.202003414.
[61] M.O. Senge, T.P. Forsyth, K. Smith, Crystal and molecular structures of some mono-meso-substituted free base and zinc(II)octaalkylporphyrins, Z. Kristallogr. 211 (1996) 176–185, https://doi.org/10.1524/zkri.1996.211.3.176.
[62] M.O. Senge, C.J. Medforth, T.P. Forsyth, D.A. Lee, M.M. Olmstead, W. Jentzen, R. K. Pandey, J.A. Shelnutt, K.M. Smith, Comparative analysis of the conformations of symmetrically and asymmetrically decaand undecasubstituted porphyrins bearing meso-alkyl or -aryl groups, Inorg. Chem. 36 (1997) 1149–1163, https://doi.org/10.1021/ic961156w.
[63] C. Krieger, M. Dernbach, G. Voit, T. Carell, H.A. Staab, Conformational mobility and crystal structures of porphyrin-quinone cyclophanes, Chem. Ber. 126 (1993) 811–821, https://doi.org/10.1002/cber.19931260336.
[64] C.J. Kingsbury, K.J. Flanagan, H.-G. Eckhardt, M. Kielmann, M.O. Senge, Weak interactions and conformational changes in core-protonated A2- and Ax-type porphyrin dications, Molecules 25 (2020) 3195, https://doi.org/10.3390/molecules25143195.
[65] M.O. Senge, 5,15-Bis(4-pentyloxyphenyl)porphyrin, Acta Cryst. E69 (2013), https://doi.org/10.1107/S160053681301550X.
[66] A.D. Bond, N. Feeder, J.E. Redman, S.J. Teat, J.K.M. Sanders, Molecular conformation and intermolecular interactions in the crystal structures of free-base 5,15-diarylporphyrins, Cryst. Growth Des. 2 (2002) 27–39, https://doi.org/10.1021/cg010029u.
[67] S. Juillard, Y. Ferrand, G. Simonneaux, L. Toupet, Molecular structure of simple mono- and diphenyl meso-substituted porphyrin diacids: influence of protonation and substitution on the distorsion, Tetrahedron 61 (2005) 3489–3495, https://doi.org/10.1016/j.tet.2005.01.128.
[68] E.G.A. Notaras, M. Fazekas, J.J. Doyle, W.J. Blau, M.O. Senge, A2B2-type push-pull porphyrins as reverse saturable and saturable absorbers, Chem. Commun. (2007) 2166–2168, https://doi.org/10.1039/b618996b.
[69] Y. Mizuno, T. Aida, K. Yamaguchi, Chirality-memory molecule: crystallographic and spectroscopic studies on dynamic molecular

recognition events by fully substituted chiral porphyrins, J. Am. Chem. Soc. 122 (2000) 5278–5285, https://doi.org/10.1021/ja000052o.
[70] J. Labuta, S. Ishihara, T. Šikorský, Z. Futera, A. Shundo, L. Hanyková, J.V. Burda, K. Ariga, J.P. Hill, NMR spectroscopic detection of chirality and enantiopurity in referenced systems without formation of diastereomers, Nat. Commun. 4 (2013) 1–8, https://doi.org/10.1038/ncomms3188.
[71] J. Labuta, J.P. Hill, S. Ishihara, L. Hanyková, K. Ariga, Chiral sensing by nonchiral tetrapyrroles, Acc. Chem. Res. 48 (2015) 521–529, https://doi.org/10.1021/acs.accounts.5b00005.
[72] V. Borovkov, Supramolecular chirality in porphyrin chemistry, Symmetry 6 (2014) 256–294, https://doi.org/10.3390/sym6020256.
[73] D.W.M. Hofmann, L.N. Kuleshova, Data Mining in Crystallography, Springer, Berlin Heidelberg, Berlin, Heidelberg, 2010.
[74] C.R. Groom, I.J. Bruno, M.P. Lightfoot, S.C. Ward, The Cambridge structural database, Acta Cryst. B 72 (2016) 171–179, https://doi.org/10.1107/S2052520616003954.
[75] J.A. Shelnutt, Normal-coordinate structural decomposition and the vibronic spectra of porphyrins, J. Porphyrins Phthalocyanines 5 (2001) 300–311, https://doi.org/10.1002/jpp.320.
[76] E.B. Fleischer, C.K. Miller, L.E. Webb, Crystal and molecular structures of some metal tetraphenylporphines, J. Am. Chem. Soc. 86 (1964) 2342–2347, https://doi.org/10.1021/ja01066a009.
[77] A.J. Hanson, The quaternion-based spatial-coordinate and orientation-frame alignment problems, Acta Cryst. A 76 (2020) 432–457, https://doi.org/10.1107/S2053273320002648.
[78] H.W. Kuhn, The Hungarian method for the assignment problem, Nav. Res. Logist. Q. 2 (1955) 83–97, https://doi.org/10.1002/nav.3800020109.
[79] S.J. Ainsworth, John A. Shelnutt, Chem. Eng. News 92 (2014) 33.
[80] M. Janssen, Y. Charalabidis, A. Zuiderwijk, Benefits, adoption barriers and myths of open data and open government, Inf. Syst. Manag. 29 (2012) 258–268, https://doi.org/10.1080/10580530.2012.716740.
[81] S. Van der Walt, M. Aivazis, The NumPy array: a structure for efficient numerical computation, Comput. Sci. Eng. 13 (2011) 22–30, https://doi.org/10.1109/MCSE.2011.37.
[82] P. Virtanen, R. Gommers, T.E. Oliphant, M. Haberland, T. Reddy, D. Cournapeau, E. Burovski, P. Peterson, W. Weckesser, J. Bright, S.J. van der Walt, M. Brett, J. Wilson, K.J. Millman, N. Mayorov, A.R.J. Nelson, E. Jones, R. Kern, E. Larson, C.J. Carey, İ. Polat, Y. Feng, E.W. Moore, J. VanderPlas, D. Laxalde, J. Perktold, R. Cimrman, I. Henriksen, E.A. Quintero, C.R. Harris, A.M. Archibald, A.H. Ribeiro, F. Pedregosa, P. van Mulbregt, A. Vijaykumar, A. Pietro Bardelli, A. Rothberg, A. Hilboll, A. Kloeckner, A. Scopatz, A. Lee, A. Rokem, C.N. Woods, C. Fulton, C. Masson, C. Häggström, C. Fitzgerald, D.A. Nicholson, D.R. Hagen, D. V. Pasechnik, E. Olivetti, E. Martin, E. Wieser, F. Silva, F. Lenders, F. Wilhelm, G. Young, G.A. Price, G.L. Ingold, G.E. Allen, G.R. Lee, H. Audren, I. Probst, J.P. Dietrich, J. Silterra, J.T. Webber, J. Slavič, J. Nothman, J. Buchner, J. Kulick, J.L. Schönberger, J.V. de Miranda Cardoso, J. Reimer, J. Harrington, J.L.C. Rodríguez, J. Nunez-Iglesias, J. Kuczynski, K. Tritz, M. Thoma, M. Newville, M. Kümmerer, M. Bolingbroke, M. Tartre, M. Pak, N.J. Smith, N. Nowaczyk, N. Shebanov, O. Pavlyk, P.A. Brodtkorb, P. Lee, R.T. McGibbon, R. Feldbauer, S. Lewis, S. Tygier, S. Sievert, S. Vigna, S. Peterson, S. More, T. Pudlik, T. Oshima, T.J. Pingel, T.P. Robitaille, T. Spura, T.R. Jones, T. Cera, T. Leslie, T. Zito, T. Krauss, U. Upadhyay, Y.O. Halchenko, Y. Vázquez-Baeza, SciPy 1.0: fundamental algorithms for scientific computing in Python, Nat. Methods. 17 (2020) 261–272. DOI:10.1038/s41592-019-0686-2..
[83] J.D. Hunter, Matplotlib: a 2D graphics environment, Comput. Sci. Eng. 9 (2007) 99–104, https://doi.org/10.1109/MCSE.2007.55.
[84] W. McKinney, Data Structures for Statistical Computing in Python, Proc. 9th Python Sci. Conf. 1697900 (2010) 51–56. http://conference.scipy.org/proceedings/scipy2010/mckinney.html..
[85] A. Ronacher, Flask, (2020). https://palletsprojects.com/p/flask/..
[86] C.F. Macrae, I. Sovago, S.J. Cottrell, P.T.A. Galek, P. McCabe, E. Pidcock, M. Platings, G.P. Shields, J.S. Stevens, M. Towler, P.A. Wood, Mercury 4.0: from visualization to analysis, design and prediction, J. Appl. Cryst. 53, (2020) 226–235. DOI:10.1107/S1600576719014092..
[87] RCSB PDB, Protein Data Bank, (2020). https://www.rcsb.org/pages/download_features#Ligands (accessed April 4, 2020)..
[88] H.M. Berman, J. Westbrook, Z. Feng, G. Gilliland, T.N. Bhat, H. Weissig, I.N. Shindyalov, P.E. Bourne, The Protein Data Bank, Nucl. Acids Res. 28 (2000) 235–242. DOI:10.1093/nar/28.1.235..
[89] Plotly Technologies Inc., Collaborative data science, (2015). https://plot.ly..
[90] I.J. Bruno, J.C. Cole, P.R. Edgington, M. Kessler, C.F. Macrae, P. McCabe, J. Pearson, R. Taylor, New software for searching the Cambridge Structural Database and visualizing crystal structures, Acta Cryst. B 58 (2002) 389–397, https://doi.org/10.1107/S0108768102003324.
[91] B.W. Silverman, Density Estimation for Statistics and Data Analysis, 1st ed., Chapman & Hall / CRC, London, 1986.
[92] M.O. Senge, A conformational study of 5,10,15,20-Tetraalkyl-22H+,24H+-porphyrindiium Salts (Dication Salts), Z. Naturforsch. 55b (2000) 336–344, https://doi.org/10.1515/znb-2000-3-417.
[93] M.O. Senge, W. W. Kalisch, Structure and conformation of tetra-meso-, octa-beta-, and dodecasubstituted 22,24-dihydroporphyrins (porphyrin dications), Z. Naturforsch. 54b (1999) 943–959. DOI:10.1515/znb-1999-0719..
[94] W. Auwärter, D. Ecija, F. Klappenberberg, J.V. Barth, Porphyrins at interfaces, Nat. Chem. 7 (2015) 105–120, https://doi.org/10.1038/nchem.2159.
[95] J. Schindler, S. Kupfer, A.A. Ryan, K.J. Flanagan, M.O. Senge, B. Dietzek, Sterically induced distortions of nickel(II) porphyrins – comprehensive investigation by DFT calculations and resonance Raman spectroscopy, Coord. Chem. Rev. 360 (2018) 1–16, https://doi.org/10.1016/j.ccr.2017.12.014.
[96] K.M. Kane, F.R. Lemke, J.L. Petersen, Trans-Difluorosilicon(IV) Complexes of Tetra-p-tolylporphyrin and Tetrakis(p-(trifluoromethyl)phenyl)porphyrin: crystal structures and unprecedented reactivity in hexacoordinate difluorosilanes, Inorg. Chem. 36 (1997) 1354–1359, https://doi.org/10.1021/ic960639x.
[97] J.Y. Zheng, K. Konishi, T. Aida, Crystallographic studies of organosilicon porphyrins: stereoelectronic effects of axial groups on the nonplanarity of the porphyrin ring, Inorg. Chem. 37 (1998) 2591–2594, https://doi.org/10.1021/ic971266i.
[98] J.A. Cissell, T.P. Vaid, A.L. Rheingold, An antiaromatic porphyrin complex: Tetraphenylporphyrinato(silicon)(L)2 (L = THF or Pyridine), J. Am. Chem. Soc. 127 (2005) 12212–12213, https://doi.org/10.1021/ja0544713.
[99] A. Yamamoto, W. Satoh, Y. Yamamoto, K.Y. Akiba, Phosphorus octaethyltetraphenylporphyrins [(oetpp)P(Me)(X)]PF6 (X = Me, OH, F) having saddle (X = Me) or ruffled (X = OH, F) conformations, Chem. Commun. 6 (1999) 147–148, https://doi.org/10.1039/a809601e.
[100] H.J. Lin, S.S. Tang, C.C. Lin, J.H. Chen, Molecular-Structure of bis(Ethane-1,2-diolato)(Tetraphenylporphyrinato)phosphorus(V) chloride: [P(tpp)(OCH2CH2OH)2]+Cl-, Aust. J. Chem. 48 (1995) 1367–1372, https://doi.org/10.1071/CH9951367.
[101] K.Y. Akiba, R. Nadano, W. Satoh, Y. Yamamoto, S. Nagase, Z. Ou, X. Tan, K.M. Kadish, Synthesis, structure, electrochemistry, and spectroelectrochemistry of hypervalent phosphorus(V) octaethylporphyrins and theoretical analysis of the nature of the PO bond in P(OEP)(CH2CH3)(O), Inorg. Chem. 40 (2001) 5553–5567, https://doi.org/10.1021/ic010595e.
[102] P.J. Nichols, G.D. Fallon, B. Moubaraki, K.S. Murray, B.O. West, The redox synthesis, structure and magnetic properties of the heterobimetallic μ-oxo compound [(py)(TPP)CrOFe(tmtaa)], Polyhedron 12 (1993) 2205–2213, https://doi.org/10.1016/S0277-5387(00)88258-3.
[103] T. Huang, X. Wu, W.W. Weare, R.D. Sommer, Mono-oxido-bridged heterobimetallic and heterotrimetallic compounds containing titanium(IV) and chromium(III), Eur. J. Inorg. Chem. 2014 (2014) 5662–5674, https://doi.org/10.1002/ejic.201402800.
[104] M. Inamo, M. Hoshino, K. Nakajima, S. Aizawa, S. Funahashi, Reactivity of five-coordinate intermediate generated by laser photolysis of monoligated Chloro(5,10,15,20-tetraphenylporphinato)chromium(III) in Toluene, Bull. Chem. Soc. Jpn. 68 (1995) 2293–2303, https://doi.org/10.1246/bcsj.68.2293.
[105] K.M. Kadish, Z. Ou, X. Tan, W. Satoh, Y. Yamamoto, K. ya Akiba, Electrochemistry and spectral characterization of arsenic porphyrins with σ-bonded axial ligands. X-ray crystallographic analysis of [(OEP)As(F)2]+PF6-, [(OEP)As(CH3)(OCH3)]+ ClO4- and [(OEP)As(C2H5)2]+PF6-, J. Porphyrins Phthalocyanines 6 (2002) 325–335, https://doi.org/10.1142/s1088424602000385.
[106] W. Satoh, R. Nadano, Y. Yamamoto, K.Y. Akiba, First characterization of arsenic porphyrins: synthesis and X-ray structure of [(oep)AsMe(OH)]+ClO4-, Chem. Commun. (1996) 2451–2452, https://doi.org/10.1039/cc9960002451.
[107] R.W.Y. Sun, C.K.L. Li, D.L. Ma, J.J. Yan, C.N. Lok, C.H. Leung, N. Zhu, C.M. Che, Stable anticancer gold(III)-porphyrin complexes: effects of porphyrin structure, Chem. Eur. J. 16 (2010) 3097–3113, https://doi.org/10.1002/chem.200902741.
[108] T.J. Foley, K.A. Abboud, J.M. Boncella, Synthesis of Ln(III) chloride tetraphenylporphyrin complexes, Inorg. Chem. 41 (2002) 1704–1706, https://doi.org/10.1021/ic015612e.
[109] X. Zhu, W.K. Wong, J. Guo, W.Y. Wong, J.P. Zhang, Reactivity of cationic lanthanide(III) monoporphyrinates towards anionic cyanometallates - preparation, crystal structure, and luminescence properties of cyanido-bridged di- and trinuclear d-f complexes, Eur. J. Inorg. Chem. (2008) 3515–3523, https://doi.org/10.1002/ejic.200800192.
[110] F. Gao, M.X. Yao, Y.Y. Li, Y.Z. Li, Y. Song, J.L. Zuo, Syntheses, structures, and magnetic properties of seven-coordinate lanthanide porphyrinate or phthalocyaninate complexes with Kläui's tripodal ligand, Inorg. Chem. 52 (2013) 6407–6416, https://doi.org/10.1021/ic400245n.
[111] H. He, X. Zhu, A. Hou, J. Guo, W.K. Wong, W.Y. Wong, K.F. Li, K.W. Cheah, Reactivity of aqua coordinated monoporphyrinate lanthanide complexes: synthetic, structural and photoluminescent studies of lanthanide porphyrinate dimers, Dalton Trans. (2004) 4064–4073, https://doi.org/10.1039/b410600h.
[112] R. Wang, R. Li, Y. Li, X. Zhang, P. Zhu, P.C. Lo, D.K.P. Ng, N. Pan, C. Ma, N. Kobayashi, J. Jiang, Controlling the nature of mixed (phthalocyaninato)(porphyrinato) rare-earth(III) double-decker complexes: the effects of nonperipheral alkoxy substitution of the phthalocyanine ligand, Chem. Eur. J. 12 (2006) 1475–1485, https://doi.org/10.1002/chem.200500733.
[113] T.E. Clement, L.T. Nguyen, R.G. Khoury, D.J. Nurco, K.M. Smith, Syntheses and structural properties of severely distorted porphyrins: N-methyl derivatives, Heterocycles 45 (1997) 651–658, https://doi.org/10.3987/COM-97-7754.
[114] J.P. Mahy, P. Battioni, G. Bedi, D. Mansuy, J. Fischer, R. Weiss, I. Morgenstern-Badarau, Iron-porphyrin-nitrene complexes: preparation, properties, and crystal structure of porphyrin-iron(III) complexes with a tosylnitrene inserted into an iron-nitrogen bond, Inorg. Chem. 27 (1988) 353–359, https://doi.org/10.1021/ic00275a024.
[115] A.L. Balch, Y.W. Chan, M. Olmstead, M.W. Renner, Structure of octaethylporphyrin N-Oxide and the characterization of its nickel(II) and copper(II) complexes, J. Am. Chem. Soc. 107 (1985) 2393–2398, https://doi.org/10.1021/ja00294a033.

[116] S. Banerjee, M. Zeller, C. Brückner, MTO/H2O2/pyrazole-mediated N-oxidation of meso-tetraarylporphyrins and -chlorins, and S-oxidation of a meso-tetraaryldithiaporphyrin and -chlorin, J. Org. Chem. 74 (2009) 4283–4288, https://doi.org/10.1021/jo9005443.
[117] M. V. Volostnykh, M.A. Mikhaylov, A.A. Sinelshchikova, G.A. Kirakosyan, A.G. Martynov, M.S. Grigoriev, D.A. Piryazev, A.Y. Tsivadze, M.N. Sokolov, Y.G. Gorbunova, Hybrid organic-inorganic supramolecular systems based on a pyridine end-decorated molybdenum(II) halide cluster and zinc(II) porphyrinate, Dalton Trans. 48 (2019) 1835–1842. DOI:10.1039/c8dt04452j..
[118] M. Čepič, Chirality, chirality transfer and the chiroclinic effect, Mol. Cryst. Liq. Cryst. 475 (2007) 151–161, https://doi.org/10.1080/15421400701681141.
[119] B.S. Everitt, S. Landau, M. Leese, D. Stahl, Cluster Analysis, 5th Edition., John Wiley & Sons Inc, Chichester, West Sussex, UK, 2011.
[120] A.C. Rencher, W.F. Christensen, Methods of Multivariate Analysis, Third Edition., John Wiley & Sons Inc, Hoboken, New Jersey, USA, 2012.
[121] S.A. MacGowan, M.O. Senge, Contribution of bacteriochlorophyll conformation to the distribution of site-energies in the FMO protein, Biochim. Biophys. Acta - Bioenerg. 2016 (1857) 427–442, https://doi.org/10.1016/j.bbabio.2016.02.001.
[122] G.N. Ramachandran, V. Sasisekharan, Conformation of polypeptides and proteins, Adv. Protein Chem. 23 (1968) 283–437, https://doi.org/10.1016/S0065-3233(08)60402-7.
[123] R.J. Anderson, Z. Weng, R.K. Campbell, X. Jiang, Main-chain conformational tendencies of amino acids, Proteins Struct. Funct. Genet. 60 (2005) 679–689, https://doi.org/10.1002/prot.20530.
[124] J.-H. Fuhrhop, L. Witte, W.S. Sheldrick, Darstellung, Struktur und Reaktivität hochsubstituierter Porphyrine, Liebigs Ann. Chem. 1976 (1976) 1537–1559, https://doi.org/10.1002/jlac.197619760904.
[125] M.O. Senge, W.W. Kalisch, S. Runge, N-Methyl derivatives of highly substituted porphyrins - The combined influence of both core and peripheral substitution on the porphyrin conformation, Liebigs Ann. 1997 (1997) 1345–1352, https://doi.org/10.1002/jlac.199719970710.
[126] G.M. MacLaughlin, Crystal and molecular structure of a non-metallo, N-substituted porphyrin, 21-ethoxycarbonylmethyl-2,3,7,8,12,13,17,18-octaethylporphyrin, J. Chem. Soc., Perkin Trans. 2 (1974) (1974) 136–140, https://doi.org/10.1039/P29740000136.
[127] T.Y. Chien, H.Y. Hsieh, C.Y. Chen, J.H. Chen, S.S. Wang, J.Y. Tung, Metal complexes of tetradentate and pentadentate N-o-hydroxybenzamido-meso-tetraphenylporphyrin ligand: M(N-NCO(o-OH)C6H4-tpp) (M = Zn2+, Ni2+, Cu2+) and M′(N-NCO(o-O) C6H4-tpp) (M′ = Mn3+) (tpp = 5, 10, 15, 20-tetraphenylporphyrinate), Polyhedron 28 (2009) 3907–3914, https://doi.org/10.1016/j.poly.2009.09.009.
[128] Kingsbury, J. Christopher, Senge, Mathias O. The Shape of Porphyrins - Normal Structural Decomposition Mendeley Data, (2020), V1, https://doi.org/10.17632/dcmtygbpyj.1.
[129] S. Sugawara, M. Kodama, Y. Hirata, S. Kojima, Y. Yamamoto, Synthesis and characterization of the most distorted 16π porphyrin: 16π octaisopropyltetraphenylporphyrin (OiPTPP), J. Porphyrins Phthalocyanines 15 (2011) 1326–1334, https://doi.org/10.1142/S1088424611004233.
[130] D.J. Nurco, C.J. Medforth, T.P. Forsyth, M.M. Olmstead, K.M. Smith, Conformational flexibility in dodecasubstituted porphyrins, J. Am. Chem. Soc. 118 (1996) 10918–10919, https://doi.org/10.1021/ja962164e.
[131] A. Krivokapic, A.R. Cowley, H.L. Anderson, Contracted and expanded meso-alkynyl porphyrinoids: from triphyrin to hexaphyrin, J. Org. Chem. 68 (2003) 1089–1096, https://doi.org/10.1021/jo026748c.
[132] T. Chandra, B.J. Kraft, J.C. Huffman, J.M. Zaleski, Synthesis and structural characterization of porphyrinic enediynes: geometric and electronic effects on thermal and photochemical reactivity, Inorg. Chem. 42 (2003) 5158–5172, https://doi.org/10.1021/ic030035a.
[133] M. Kielmann, N. Grover, W.W. Kalisch, M.O. Senge, Incremental introduction of organocatalytic activity into conformationally engineered porphyrins, Eur. J. Org. Chem. 2019 (2019) 2448–2452, https://doi.org/10.1002/ejoc.201801691.
[134] P. Ochsenbein, K. Ayougou, D. Mandon, J. Fischer, R. Weiss, R.N. Austin, K. Jayaraj, A. Gold, J. Terner, J. Fajer, Conformational effects on the redox potentials of tetraarylporphyrins halogenated at the β-pyrrole positions, Angew. Chem., Int. Ed. Engl. 33 (1994) 348–350, https://doi.org/10.1002/anie.199403481.
[135] C.J. Medforth, M.O. Senge, T.P. Forsyth, J.D. Hobbs, J.A. Shelnutt, K.M. Smith, Conformational study of 2,3,5,7,8,12,13,15,17,18-decaalkylporphyrins, Inorg. Chem. 33 (1994) 3865–3872, https://doi.org/10.1021/ic00096a008.
[136] M.O. Senge, Database of Tetrapyrrole Crystal Structure Determinations. In: K. M. Kadish, K.M. Smith, R. Guilard (Eds.), The Porphyrin Handbook, Vol. 10, Academic Press, San Diego, pp. 1–218. ISBN: 978-0080923833..
[137] J. Herritsch, J.-N. Luy, S. Rohlf, M. Gruber, B.P. Klein, M. Kalläne, P. Schweyen, M. Bröring, K. Rossnagel, R. Tonner, J.M. Gottfried, Influence of ring contraction on the electronic structure of nickel tetrapyrrole complexes: corrole vs porphyrin, ECS J. Solid State Sci. Technol. 9 (2020), https://doi.org/10.1149/2162-8777/ab9e18.
[138] J.A. Shelnutt, C.J. Medforth, M.D. Berber, K.M. Barkigia, K.M. Smith, Relationships between structural parameters and Raman frequencies for some planar and nonplanar nickel(II) porphyrins, J. Am. Chem. Soc. 113 (1991) 4077–4087, https://doi.org/10.1021/ja00011a004.
[139] J.A. Shelnutt, S.A. Majumder, L.D. Sparks, J.D. Hobbs, C.J. Medforth, M.O. Senge, K.M. Smith, M. Miura, L. Luo, J.M.E. Quirke, Resonance Raman spectroscopy of non-planar nickel porphyrins, J. Raman Spectrosc. 23 (1992) 523–529, https://doi.org/10.1002/jrs.1250231004.
[140] M.O. Senge, M. Davis, (5,15-Dianthracen-9-yl-10,20-dihexylporphyrinato) nickel(II): a planar nickel(II) porphyrin, Acta Cryst. 66 (2010), https://doi.org/10.1107/S1600536810021434.
[141] M.O. Senge, T. Ema, K.M. Smith, Crystal structure of a remarkably ruffled nonplanar porphyrin (pyridine)[5,10,15,20-tetra(tert-butyl)porphyrinato] zinc(II), J. Chem. Soc., Chem. Commun. 165 (1995) 733, https://doi.org/10.1039/c39950000733.
[142] K.E. Thomas, C. Slebodnick, A. Ghosh, Facile supramolecular engineering of porphyrin cis tautomers: the case of β-octabromo- meso-tetraarylporphyrins, ACS Omega 5 (2020) 8893–8901, https://doi.org/10.1021/acsomega.0c00517.
[143] P. Bhyrappa, K. Karunanithi, Porphyrin-fullerene, C60, cocrystallates: influence of C60 on the porphyrin ring conformation, Inorg. Chem. 49 (2010) 8389–8400, https://doi.org/10.1021/ic101030h.
[144] W. Suzuki, H. Kotani, T. Ishizuka, T. Kojima, Dioxygen/hydrogen peroxide interconversion using redox couples of saddle-distorted porphyrins and isophlorins, J. Am. Chem. Soc. 141 (2019) 5987–5994, https://doi.org/10.1021/jacs.9b01038.
[145] M. Ravikanth, T.K. Chandrashekar. Nonplanar porphyrins and their biological relevance: Ground and excited state dynamics. In: Coordination Chemistry, Structure and Bonding, vol 82. Springer, Berlin, Heidelberg. ISBN 978-3-540-58761-3 (1995) DOI:10.1007/BFb0036827..
[146] Eratosthenes, On the Measurement of the Earth, (original work published ca. 240 B.C.E.) described in: G. Sarton, A History of Science. Ancient science through the Golden Age of Greece, Harvard University Press, Cambridge, Massachusetts, 1952..
[147] Y. Bian, J. Jiang, Y. Tao, M.T.M. Choi, R. Li, A.C.H. Ng, P. Zhu, N. Pan, X. Sun, D.P. Arnold, Z.Y. Zhou, H.W. Li, T.C.W. Mak, D.K.P. Ng, Tuning the valence of the cerium center in (Na)phthalocyaninato and porphyrinato cerium double-deckers by changing the nature of the tetrapyrrole ligands, J. Am. Chem. Soc. 125 (2003) 12257–12267, https://doi.org/10.1021/ja036017+.
[148] M. Umetani, K. Naoda, T. Tanaka, S.K. Lee, J. Oh, D. Kim, A. Osuka, Synthesis of di-peri-dinaphthoporphyrins by PtCl2-mediated cyclization of quinodimethane-type porphyrins, Angew. Chem. Int. Ed. 55 (2016) 6305–6309, https://doi.org/10.1002/anie.201601303.
[149] H. Zhang, H. Phan, T.S. Herng, T.Y. Gopalakrishna, W. Zeng, J. Ding, J. Wu, Conformationally flexible Bis(9-fluorenylidene)porphyrin diradicaloids, Angew. Chem. Int. Ed. 56 (2017) 13484–13488, https://doi.org/10.1002/anie.201707480.
[150] M.O. Senge, S. Runge, M. Speck, K. Ruhlandt-Senge, Identification of stable porphomethenes and porphodimethenes from the reaction of sterically hindered aldehydes with pyrrole, Tetrahedron 56 (2000) 8927–8932, https://doi.org/10.1016/S0040-4020(00)00823-1.
[151] P.N. Dwyer, L. Puppe, J.W. Buchler, R. Scheidt, Molecular stereochemistry of (α, γ-Dimethyl- α, γ-dihydrooctaethylporphinato)oxotitanium(IV), Inorg. Chem. 14 (1975) 1782–1785, https://doi.org/10.1021/ic50150a008.
[152] A.L. Balch, M.M. Olmstead, Reactions of transition metal complexes with fullerenes (C60, C70, etc.) and related materials, Chem. Rev. 98 (1999) 2123–2165, https://doi.org/10.1021/cr960040e.
[153] M. Roy, M.M. Olmstead, A.L. Balch, Metal ion effects on fullerene/porphyrin cocrystallization, Cryst. Growth Des. 19 (2019) 6743–6751, https://doi.org/10.1021/acs.cgd.9b01092.
[154] M.M. Olmstead, D.A. Costa, K. Maitra, B.C. Noll, S.L. Philipps, P.M. Van Calcar, A.L. Balch, Interaction of curved and flat molecular surfaces. The structures of crystalline compounds composed of fullerene (C60, C60O, C70, and C120O) and metal octaethylporphyrin units, J. Am. Chem. Soc. 21 (1999) 7090–7097, https://doi.org/10.1021/ja990618c.
[155] D.V. Konarev, S.S. Khasanov, G. Saito, R.N. Lyubovskaya, Design of molecular and ionic complexes of fullerene C60 with Metal(II) octaethylporphyrins, MIIOEP (M = Zn Co, Fe, and Mn) containing coordination M−N(ligand) and M−C(C60−) bonds, Cryst. Growth Des. 9 (2009) 1170–1181, https://doi.org/10.1021/cg8010184.
[156] A. Takenaka, Y. Sasada, H. Ogoshi, T. Omura, Z. Yoshida, The crystal and molecular structure of μ-1,2,3,4,5,6,7,8-octaethylporphinatobis [dicarbonylrhodium(I)], Acta Cryst. B 31 (1975) 1–6, https://doi.org/10.1107/S0567740875001999.
[157] P.J. Brothers, Boron complexes of porphyrins and related polypyrrole ligands: Unexpected chemistry for both boron and the porphyrin, Chem. Commun. (2008) 2090–2102. DOI:10.1039/b714894a..
[158] A. Srinivasan, H. Furuta, A. Osuka, The first bis-Rh(I) metal complex of N-confused porphyrin, Chem. Commun. (2001) 1666–1667, https://doi.org/10.1039/b104004a.
[159] Y. Mizuno, M.A. Alam, A. Tsuda, K. Kinbara, K. Yamaguchi, T. Aida, Hermaphroditic chirality of a D2-symmetric saddle-shaped porphyrin in multicomponent spontaneous optical resolution: inclusion cocrystals with double-helical porphyrin arrays, Angew. Chem. Int. Ed. 45 (2006) 3786–3790, https://doi.org/10.1002/anie.200503054.
[160] M. Balaz, Y.A. Joh, K. Varga, N. Berova, R. Purrello, A. D'Urso, Structure and Electronic Circular Dichroism of Chiral Porphyrins and Chiral Porphyrin Dimers, in: K.M. Kadish, K.M. Smith, R. Guilard (Eds.), Handbook of Porphyrin Science, vol. 45, World Scientific, Singapore, 2019, pp. 205–284, https://doi.org/10.1142/9789811201813_0003.
[161] Y. Hu, K. Lang, J. Tao, M.K. Marshall, Q. Cheng, X. Cui, L. Wojtas, X.P. Zhang, Next-generation D2 -symmetric chiral porphyrins for cobalt(II)-based metalloradical catalysis: catalyst engineering by distal bridging, Angew.

Chem. Int. Ed. 58 (2019) 2670–2674, https://doi.org/10.1002/anie.201812379.
[162] Z. Gross, S. Ini, Asymmetric catalysis by a chiral ruthenium porphyrin: epoxidation, hydroxylation, and partial kinetic resolution of hydrocarbons, Org. Lett. 1 (1999) 2077–2080, https://doi.org/10.1021/ol991131b.
[163] A.M.G. Silva, K.T. De Oliveira, M.A.F. Faustino, M.G.P.M.S. Neves, A.C. Tomé, A. M.S. Silva, J.A.S. Cavaleiro, P. Brandão, V. Felix, Chemical transformations of mono- and bis(buta-1,3-dien-1-yl)porphyrins: a new synthetic approach to mono- and dibenzoporphyrins, Eur. J. Org. Chem. (2008) 704–712, https://doi.org/10.1002/ejoc.200700852.
[164] M. Luciano, W. Tardie, M. Zeller, C. Brückner, Supersizing pyrrole-modified porphyrins by reversal of the 'breaking and mending' strategy, Chem. Commun. 52 (2016) 10133–10136, https://doi.org/10.1039/C6CC04028D.
[165] D. Gibbons, K.J. Flanagan, L. Pounot, M.O. Senge, Structure and conformation of photosynthetic pigments and related compounds. 15. Conformational analysis of chlorophyll derivatives - implications for hydroporphyrins in vivo, Photochem. Photobiol. Sci. 18 (2019) 1479–1494, https://doi.org/10.1039/c8, pp00500a.
[166] S. Nakamura, S. Hiroto, H. Shinokubo, Synthesis and oxidation of cyclic tetraindole, Chem. Sci. 3 (2012) 524–527, https://doi.org/10.1039/c1sc00665g.
[167] K.M. Bergman, G.M. Ferrence, T.D. Lash, Tropiporphyrins, cycloheptatrienyl analogues of the porphyrins: synthesis, spectroscopy, chemistry, and structural characterization of a silver(III) derivative, J. Org. Chem. 69 (2004) 7888–7897, https://doi.org/10.1021/jo040213x.
[168] C. Brückner, The breaking and mending of meso-tetraarylporphyrins: transmuting the pyrrolic building blocks, Acc. Chem. Res. 49 (2016) 1080–1092, https://doi.org/10.1021/acs.accounts.6b00043.
[169] N. Kobayashi, T. Fukuda, K. Ueno, H. Ogino, extremely non-planar phthalocyanines with saddle or helical conformation: synthesis and structural characterizations, J. Am. Chem. Soc. 123 (2001) 10740–10741, https://doi.org/10.1021/ja0113753.
[170] Y. Takano, H.X. Kondo, Y. Kanematsu, Y. Imada, Computational study of distortion effect of Fe-porphyrin found as a biological active site, Jpn. J. Appl. Phys. 59 (2020), https://doi.org/10.7567/1347-4065/ab62b9.
[171] H.X. Kondo, Y. Kanematsu, G. Masumoto, Y. Takano, PyDISH: database and analysis tools for heme porphyrin distortion in heme proteins, Database (2020), https://doi.org/10.1093/database/baaa066.
[172] G. Ulrich, R. Ziessel, A. Harriman, The chemistry of fluorescent Bodipy dyes: versatility unsurpassed, Angew. Chem. Int. Ed. 47 (2008) 1184–1201, https://doi.org/10.1002/anie.200702070.
[173] A. Burghart, H.J. Kim, M.B. Welch, L.H. Thoresen, J. Reibenspies, K. Burgess, F. Bergstrom, L.B.A. Johansson, 3,5-Diaryl-4,4-difluoro-4-bora-3a,4a-diaza-s-indacene (BODIPY) dyes: synthesis, spectroscopic, electrochemical, and structural properties, J. Org. Chem. 64 (1999) 7813–7819, https://doi.org/10.1021/jo990796o.
[174] M.A. Filatov, S. Karuthedath, P.M. Polestshuk, S. Callaghan, K.J. Flanagan, M. Telitchko, T. Wiesner, F. Laqaui, M.O. Senge, Control of triplet state generation in heavy atom-free BODIPY-anthracene dyads by media polarity and structural factors, Phys. Chem. Chem. Phys. 20 (2018) 8016–8031, https://doi.org/10.1039/c7cp08472b.
[175] K.T. Butler, D.W. Davies, H. Cartwright, O. Isayev, A. Walsh, Machine learning for molecular and materials science, Nature 559 (2018) 547–555, https://doi.org/10.1038/s41586-018-0337-2.
[176] P.S. Gromski, A.B. Henson, J.M. Granda, L. Cronin, How to explore chemical space using algorithms and automation, Nat. Rev. Chem. 3 (2019) 119–128, https://doi.org/10.1038/s41570-018-0066-y.
[177] J.D. Bourke, M.T. Islam, S.P. Best, C.Q. Tran, F. Wang, C.T. Chantler, conformation analysis of ferrocene and decamethylferrocene via full-potential modeling of XANES and XAFS spectra, J. Phys. Chem. Lett. 7 (2016) 2792–2796, https://doi.org/10.1021/acs.jpclett.6b01382.